The Plant Cell, Vol. 20: 101–123, January 2008, www.plantcell.org

Rab-A2 and Rab-A3 GTPases Define a *trans*-Golgi Endosomal Membrane Domain in *Arabidopsis* That Contributes Substantially to the Cell Plate [W]

Cheung-Ming Chow, Hélia Neto, Camille Foucart, and Ian Moore[1]

Department of Plant Sciences, University of Oxford, Oxford OX1 3RB, United Kingdom

The Ypt3/Rab11/Rab25 subfamily of Rab GTPases has expanded greatly in *Arabidopsis thaliana*, comprising 26 members in six provisional subclasses, Rab-A1 to Rab-A6. We show that the Rab-A2 and Rab-A3 subclasses define a novel post-Golgi membrane domain in *Arabidopsis* root tips. The Rab-A2/A3 compartment was distinct from but often close to Golgi stacks and prevacuolar compartments and partly overlapped the VHA-a1 *trans*-Golgi compartment. It was also sensitive to brefeldin A and accumulated FM4-64 before prevacuolar compartments did. Mutations in RAB-A2^a that were predicted to stabilize the GDP- or GTP-bound state shifted the location of the protein to the Golgi or plasma membrane, respectively. In mitosis, KNOLLE accumulated principally in the Rab-A2/A3 compartment. During cytokinesis, Rab-A2 and Rab-A3 proteins localized precisely to the growing margins of the cell plate, but VHA-a1, GNOM, and prevacuolar markers were excluded. Inducible expression of dominant-inhibitory mutants of RAB-A2^a resulted in enlarged, polynucleate, meristematic cells with cell wall stubs. The Rab-A2/A3 compartment, therefore, is a *trans*-Golgi compartment that communicates with the plasma membrane and early endosomal system and contributes substantially to the cell plate. Despite the unique features of plant cytokinesis, membrane traffic to the division plane exhibits surprising molecular similarity across eukaryotic kingdoms in its reliance on Ypt3/Rab11/Rab-A GTPases.

INTRODUCTION

The organization of membrane traffic in plants is comparatively poorly understood but exhibits several unique features (Boevink et al., 1998; Rutherford and Moore 2002; Jürgens, 2004, 2005; Richter et al., 2007; Teh and Moore, 2007). Recent interest has focused on endocytic recycling pathways that play important roles in the maintenance of cell polarity (Moore, 2002; Geldner, 2004; Jaillais et al., 2007). There is still uncertainty about the organization of the endosomal compartments and prevacuolar compartments (PVCs) and the trafficking routes between them. Compartments labeled by small GTPases of the Rab-F1 (ARA6) and Rab-F2 (ARA7/RHA1) subclasses have been viewed as early endosomes (EEs) and PVCs (Geldner, 2004; Kotzer et al., 2004; Lee et al., 2004; Ueda et al., 2004; Haas et al., 2007; Jaillais et al., 2007), while GNOM defines another endosome involved in recycling to the plasma membrane (PM) (Geldner et al., 2003; Geldner, 2004; Richter et al., 2007). In *Arabidopsis thaliana*, the VHA-a1 subunit of the V-ATPase defines a *trans*-Golgi network (TGN) compartment at the intersection of secretory and early endocytic pathways (Dettmer et al., 2006). In tobacco (*Nicotiana tabacum*) BY-2 cells, tubular membranes at the *trans*-Golgi are labeled by V-ATPase and SCAMP1 and also appear to be EEs (Lam et al., 2007a, 2007b).

Cytokinesis in land plants is a unique vesicular process in which a new cell wall is deposited in an intracellular compartment, the cell plate, which expands across the division plane and fuses with the PM to externalize the nascent wall (Jürgens and Pacher, 2004). Cell plate formation can be completed in less than half an hour and generates one-third of the new surface area of the cell (Jürgens and Pacher, 2004). To account for this, it has been proposed that, before the onset of cytokinesis, cell plate components, including the cytokinesis-specific syntaxin KNOLLE (KN), are stored in a Golgi-derived compartment (Yasuhara et al., 1995; Lauber et al., 1997; Yasuhara and Shibaoka, 2000; Jürgens and Pacher, 2004). The Golgi-to-cell plate pathway is proposed to be a polarized modified version of the preexisting secretory pathway(s) (Bednarek and Falbel, 2002; Jürgens and Pacher, 2004). However, an alternative recent suggestion is that the cell plate is constructed preferentially from endocytosed polysaccharide and membrane (Baluska et al., 2005, 2006; Dhonukshe et al., 2006).

The molecular mechanisms that promote membrane trafficking through the endosomal system are still poorly understood, but phylogenetic analyses indicate that membrane trafficking mechanisms have diversified independently in plant and animal lineages (Sanderfoot et al., 2000; Rutherford and Moore, 2002; Mouratou et al., 2005). This is illustrated by analysis of the Rab GTPase family (Ypt family in yeasts). These small monomeric GTPases are important regulators of membrane targeting, identity, and fusion, with individual members localizing to specific membranes and acting in specific vesicle transport events (Segev, 2001; Zerial and McBride, 2001; Grosshans et al., 2006). Although *Arabidopsis* encodes almost as many Rab GTPases as human (57 and 70, respectively), most of the mammalian Rab subclasses are missing from the *Arabidopsis* genome

[1] Address correspondence to ian.moore@plants.ox.ac.uk.
The author responsible for distribution of materials integral to the findings presented in this article in accordance with the policy described in the Instructions for Authors (www.plantcell.org) is: Ian Moore (ian.moore@plants.ox.ac.uk).
[W] Online version contains Web-only data.
www.plantcell.org/cgi/doi/10.1105/tpc.107.052001

(Rutherford and Moore, 2002). Notable absentees are subclasses involved in regulated exocytosis (Rab3), cell polarization (Rab17), or aspects of endocytic trafficking, such as Rab9, Rab4, Rab14, Rab15, Rab20, Rab21, Rab22, and Rab24 (Rodman and Wandinger-Ness, 2000; Mouratou et al., 2005; Proikas-Cezanne et al., 2006).

Conversely, some ancestral Rab GTPases have proliferated and diversified specifically in the higher plant lineage. The most striking example is provided by the Rab-A proteins of higher plants, which are related to the animal Rab11 and Rab25 subclasses. This clade of Rab proteins is represented by a single gene in *Saccharomyces pombe* (Ypt3), by two redundant genes in *Saccharomyces cerevisiae* (Ypt31 and 32), and by three genes in human (Rab11A, Rab11B, and Rab25), yet there are 26 Rab-A proteins in *Arabidopsis* and 17 in rice (*Oryza sativa*). These proteins thus represent plant-specific paralogues (Rutherford and Moore, 2002; Vernoud et al., 2003). The 26 *Arabidopsis* Rab-A proteins have been divided into six provisional subclasses, Rab-A1 to Rab-A6, based either on overall sequence similarity (Rutherford and Moore, 2002; Vernoud et al., 2003) or on similarity in four specificity-determining regions (Pereira-Leal and Seabra, 2001).

In animals, Rab11 and Rab25 function at the recycling endosome, with Rab11 also performing an important function in the later stages of cytokinesis (Skop et al., 2001; Pelissier et al., 2003; Riggs et al., 2003; Wilson et al., 2005; van IJzendoorn, 2006). In yeast, Ypt3 and Ypt31/32 are involved in trafficking at the *trans*-face of the Golgi on the biosynthetic and endocytic pathways and localize to the site of cytokinesis (Jedd et al., 1997; Cheng et al., 2002; Pelham, 2002; Chen et al., 2005; Ortiz and Novick, 2006). Comparatively little is known about the trafficking functions of the large plant Rab-A clade (Rutherford and Moore, 2002; Vernoud et al., 2003). In tobacco pollen tubes, Nt RAB11, a member of the tobacco Rab-A1 subclass, targeted green fluorescent protein (GFP) to the vesicle-rich tip region of the tube (de Graaf et al., 2005). The same study showed that GTP binding or hydrolysis mutants of Nt RAB11 inhibited the growth of transfected pollen tubes, and a role in exocytosis was proposed. Os RAB11, a member of the rice Rab-A1 subclass, has been implicated in the trafficking of proteins from the TGN to the PM or the central vacuole, because overexpression of Os RAB11, but not of Os RAB8, relieved the inhibitory effect of the mutant proteins of Os GAP1 on the transport of PM and vacuolar cargoes from the TGN (Heo et al., 2005). A member of the *Arabidopsis* Rab-A4 subclass, RAB-A4^b, has been implicated in tip growth in root hairs via its interaction with two phosphatidylinositol-4-kinases that together are essential for root hair morphogenesis (Preuss et al., 2006). RAB-A4^b targets yellow fluorescent protein (YFP) to membranes near the *trans*-face of the Golgi stacks at the tips of elongating root hairs (Preuss et al., 2004), and RAB-A5^c (ARA4) has been immunolocalized to Golgi-associated vesicles in pollen (Ueda et al., 1996).

The targeting of individual Rab proteins to specific membranes is a key determinant of their distinct functions (Pfeffer, 2001; Munro, 2004; Seabra and Wasmeier, 2004). There is evidence that members of the pea (*Pisum sativum*) Rab-A3 and Rab-A4 subclasses (Pra2 and Pra3) are targeted to distinct organelles when expressed heterologously in BY-2 cells as GFP fusions (Inaba et al., 2002). Here, we investigate the localization and functions of the *Arabidopsis* Rab-A2 and Rab-A3 subclasses in *Arabidopsis* root tips, where the plant endosomal system has been characterized most extensively (Geldner, 2004; Dettmer et al., 2006; Richter et al., 2007; Teh and Moore, 2007).

RESULTS

Expression Patterns and Membrane Targeting of *Arabidopsis* Rab-A2 and Rab-A3 Proteins

For localization studies, we constructed YFP fusions with genomic DNA fragments from all four members of the Rab-A2 subclass (RAB-A2^a, -A2^b, -A2^c, and -A2^d) and with the single Rab-A3 protein (RAB-A3). These DNA fragments included the entire intergenic region with additional upstream sequences in some instances (see Supplemental Figure 1 online). Fluorescence microscopy of transgenic plants (see Supplemental Figure 2 online) indicated that the transgenes were expressed in a range of cell types and tissues. In brief, while *RAB-A2^c* and *-A2^d* were expressed in most cells, *RAB-A2^a* and *-A2^b* and *RAB-A3* showed more restricted expression patterns. For instance, in the root tips, *YFP:RAB-A3* was expressed exclusively in lateral root cap and epidermis, *YFP:RAB-A2^b* was strongest in the columella, and *YFP:RAB-A2^a* was strongest in the meristem. These data were consistent with the analysis of mRNA abundance at the AtGenExpress website (Schmid et al., 2005) (see Supplemental Figure 3 online). Thus, differential yet overlapping expression patterns were observed within the Rab-A2 subclass and between the Rab-A2 and Rab-A3 subclasses.

Confocal laser scanning microscopy (CLSM) of cells in the meristem and elongation zone of seedling roots revealed that each fusion predominantly labeled numerous mobile punctate structures against a faint cytosolic background, with faint labeling of the PM also occasionally visible. To determine whether the *Arabidopsis* Rab-A proteins each target YFP to the same punctate structures, we crossed these plants with plants expressing GFP:PsRAB-A3, a GFP-tagged form of Pra2, a pea Rab-A3 protein (Inaba et al., 2002; Rutherford and Moore, 2002). As shown in Figure 1A and Supplemental Figure 4 online, GFP:PsRAB-A3 colocalized with YFP fusions to each of the *Arabidopsis* RAB-A proteins. Thus, all members of the *Arabidopsis* Rab-A2 and Rab-A3 subclasses target YFP to the same compartment, which we refer to as the Rab-A2/A3 compartment.

Polyclonal antisera were raised to a peptide corresponding to the C terminus of *Arabidopsis* RAB-A2^a. Affinity-purified antibodies labeled a single band of the expected mobility (~26 kD) in extracts of wild-type roots and an additional band of ~50 kD in extracts from roots expressing YFP:RAB-A2^a (Figure 1B). Importantly, no cross reactivity was observed to other members of the RAB-A2 subclass, to RAB-A5^c, RAB-A3, RAB-A4^b, or RAB-A6^a, or to members of the Rab-B, -C1, and -E subclasses, indicating the high specificity of the antibodies (Figure 1B).

The anti-RAB-A2^a antiserum was used for indirect immunofluorescence analysis of *Arabidopsis* root meristems expressing YFP:RAB-A2^d. The anti-RAB-A2^a antibody does not cross react with RAB-A2^d (Figure 1B), consistent with the high sequence divergence between RAB-A2^a and -A2^d in the region used to

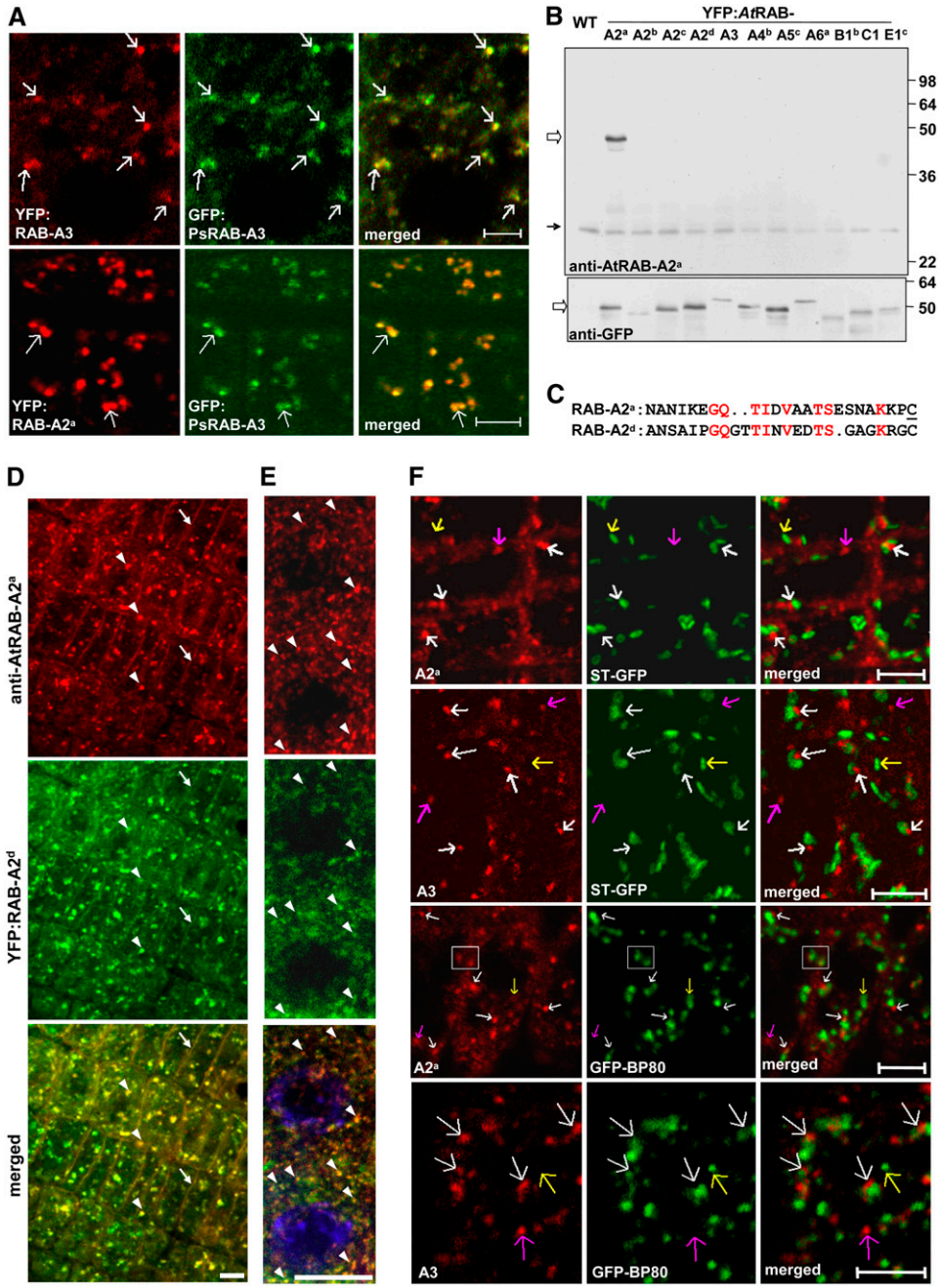

Figure 1. At RAB-A2, At RAB-A3, and Ps RAB-A3 Label the Same Compartment, Which Is Distinct from the Golgi and the GFP-BP80–Labeled PVC.

(A) CLSM analysis of seedling root tip epidermis coexpressing GFP:PsRAB-A3 (green) with YFP:RAB-A3 or YFP:RAB-A2^a (fusions to *Arabidopsis* Rab proteins) as indicated (each red). White arrows indicate examples of structures with extensive overlap of GFP and YFP signals. Bars = 5 μm.

(B) Protein gel blot analysis of total protein extracted from roots of 14-d-old seedlings of wild-type or transgenic plants expressing the indicated YFP:AtRab fusion and probed with desalted affinity-purified anti-RAB-A2^a (1:1000) (top panel) or anti-GFP (1:1000) (bottom panel). Open arrows indicate the expected sizes of YFP:AtRAB fusions (50 kD); the closed arrow indicates the expected size of endogenous At RAB-A2^a (26 kD).

(C) Sequences of At RAB-A2^a peptide antigen and the At RAB-A2^d C terminus are dissimilar. The sequences were manually aligned to maximize the number of consecutive shared amino acids. Underlining indicates the conserved Cys residue that is expected to be geranylgeranylated in the native protein and was used for coupling the peptide. The At RAB-A2^a peptide and At RAB-A2^d share only eight residues (red), and none of these residues form a contig of three residues or more.

(D) and **(E)** Immunolocalization of At RAB-A2^a (red) in root tip cells expressing YFP:AtRAB-A2^d (green). The 4′,6-Diamidino-2-phenylindole (DAPI)–stained nuclei in **(E)** are in blue. Arrowheads indicate examples of colocalizing punctate structures; arrows indicate labeling at the cell periphery. Bars = 5 μm.

generate the antigenic peptide (Figure 1C). As shown in Figures 1D and 1E, there was excellent colocalization between the antibody signal and the YFP:RAB-A2^{d} signal on punctate structures and at the cell periphery. Thus, endogenous RAB-A2^{a} also resides predominantly on the Rab-A2/A3 compartment.

The Rab-A2/A3 Compartment Is Distinct from the Golgi and PVCs

To investigate the identity of the Rab-A2/A3 compartment, plants expressing each of the YFP:RAB-A fusions were crossed with plants expressing GFP markers of the Golgi and PVC. Golgi stacks, identified by ST-GFP (Boevink et al., 1998; Zheng et al., 2004), appeared as flattened discs, often with darker regions at their centers, whereas the Rab-A2/A3 compartment was physically distinct and appeared as smaller punctae (Figure 1F; see Supplemental Figures 5A to 5D online). Although the Rab-A2/A3 compartment and Golgi stacks were often in close physical proximity and occasionally moved together in the streaming cytoplasm, their proximity was transient (see Supplemental Figure 5E online). Similarly, the Rab-A2/A3 compartment was often transiently close to but distinct from the multivesicular PVCs identified by the vacuolar sorting receptor marker GFP-BP80 (Kotzer et al., 2004; Tse et al., 2004) (Figure 1F; see Supplemental Figure 6 online). We concluded that the Rab-A2/A3 compartment is distinct from the Golgi apparatus and the PVC.

The Rab-A2/A3 Compartment Is an Early Site of FM4-64 Accumulation

In *Arabidopsis*, the lipophilic styryl dye FM4-64 is internalized via a clathrin-dependent process (Dhonukshe et al., 2007) and sequentially labels a variety of endosomal, prevacuolar, and vacuolar compartments over 1 to 2 h (Ueda et al., 2001, 2004; Bolte et al., 2004; Tse et al., 2004; Dettmer et al., 2006). It is speculated that this sequence may reflect the endocytic pathway by which the dye and other endocytosed materials are transported (Bolte et al., 2004; Dhonukshe et al., 2007). When FM4-64 was applied to root tips expressing either one of the four YFP:RAB-A2 fusions or YFP:RAB-A3, extensive colocalization was observed in epidermal cells within 4 to 6 min. The relative intensities of the FM4-64 and YFP signals varied on individual compartments, however, and some were apparently labeled by one marker only (Figures 2A and 2B; see Supplemental Figures 7A to 7D online).

GNOM is required for the recycling of some membrane proteins from an endosomal compartment, and GNOM:GFP partially localizes to FM4-64–labeled compartments (Geldner et al., 2003). We found that the extent of colocalization with FM4-64 was significantly less for GNOM:GFP than for the Rab-A2/A3 compartment even at 25 min or more after addition of the dye (cf. Figures 2A and 2B with Figure 2C and Supplemental Figures 7E and 7F online). Similarly, the GFP-BP80 PVC labeled slowly and partially with FM4-64 (see Supplemental Figures 8A to 8C online). In roots expressing both GFP-BP80 and YFP:RAB-A2^{a} or YFP:RAB-A3, it was clear that FM4-64 labeled the Rab-A2/A3 compartment prior to this PVC (Figure 2D; see Supplemental Figure 8D online). Consistent with this, FM4-64 showed relatively little colocalization with either of the two *Arabidopsis* Rab-F2 proteins that colocalize at the same PVC as vacuolar sorting receptors (Kotzer et al., 2004; Lee et al., 2004) (Figures 2E and 2F; see Supplemental Figures 7G to 7I online). Similarly, YFP fusions to Golgi-localized Rab GTPases of the Rab-E or Rab-B subclass (Cheung et al., 2002; Zheng et al., 2005) (Figures 2G and 2H; see Supplemental Figure 7J online) or the Rab-H subclass (C. Chow and I. Moore, unpublished data) (Figure 2I) showed little colocalization with FM4-64 at 20 min or more after dye application, although these structures were often in very close proximity. Thus, the Rab-A2/A3 compartment is an early site of FM4-64 accumulation within the endosomal and prevacuolar system of the *Arabidopsis* root tip.

The Rab-A2/A3 Compartment Defines a Novel *trans*-Golgi Early Endosomal Domain That Overlaps the VHA-a1 Compartment

When the FM4-64–labeled Rab-A2/A3 compartment was imaged at high resolution, it was clear that the colocalizing regions were often associated with FM4-64–labeled domains that lacked YFP:RAB-A2 or -A3 signal (Figure 2J). In time-lapse imaging, the colocalized and noncolocalized domains often remained closely associated in the streaming cytoplasm, but structures enriched in FM4-64 were also seen to separate from the colocalized region (see Supplemental Figure 9 online). By contrast, the YFP:RAB signal rarely if ever separated from the FM4-64 signal. Thus, FM4-64 appeared to label additional membranes that are in close proximity to the Rab-A2/A3 compartment.

The VHA-a1 subunit of the vacuolar V-ATPase complex marks a *trans*-Golgi compartment that is also an early site of FM4-64 accumulation (Dettmer et al., 2006). To determine the spatial relationship between the Rab-A2/A3 and VHA-a1 compartments, plants expressing YFP:RAB-A2^{a} were crossed to a VHA-a1:GFP line (Dettmer et al., 2006). Confocal images from root tips indicated that VHA-a1:GFP and YFP:RAB-A2^{a} exhibited overlapping membrane distributions (Figures 2K to 2M). Qualitative analysis of marker distribution (Figure 2N) indicated that each marker colocalized in ~35% of labeled compartments, while 30% of VHA-a1:GFP compartments and 40% of YFP:

Figure 1. (continued).

(F) CLSM analysis of seedling root tip epidermal cells coexpressing YFP:AtRAB-A2^{a} or YFP:AtRAB-A3 (red) with ST-GFP or GFP-BP80 (each green) as indicated. Yellow arrows point to the Golgi or PVC (green), which are not close to any YFP:AtRAB-A–labeled structure (red puncta). Pink arrows point to the YFP:AtRAB-A–labeled structures, which are not close to the Golgi or PVC. White arrows point to the YFP:RAB-A–labeled punctate structures, which are closely associated with the Golgi or PVCs. Occasionally, YFP:RAB-A–labeled structures and GFP-BP80-labeled PVCs partially overlap (e.g., the boxed region). Bars = 5 μm.

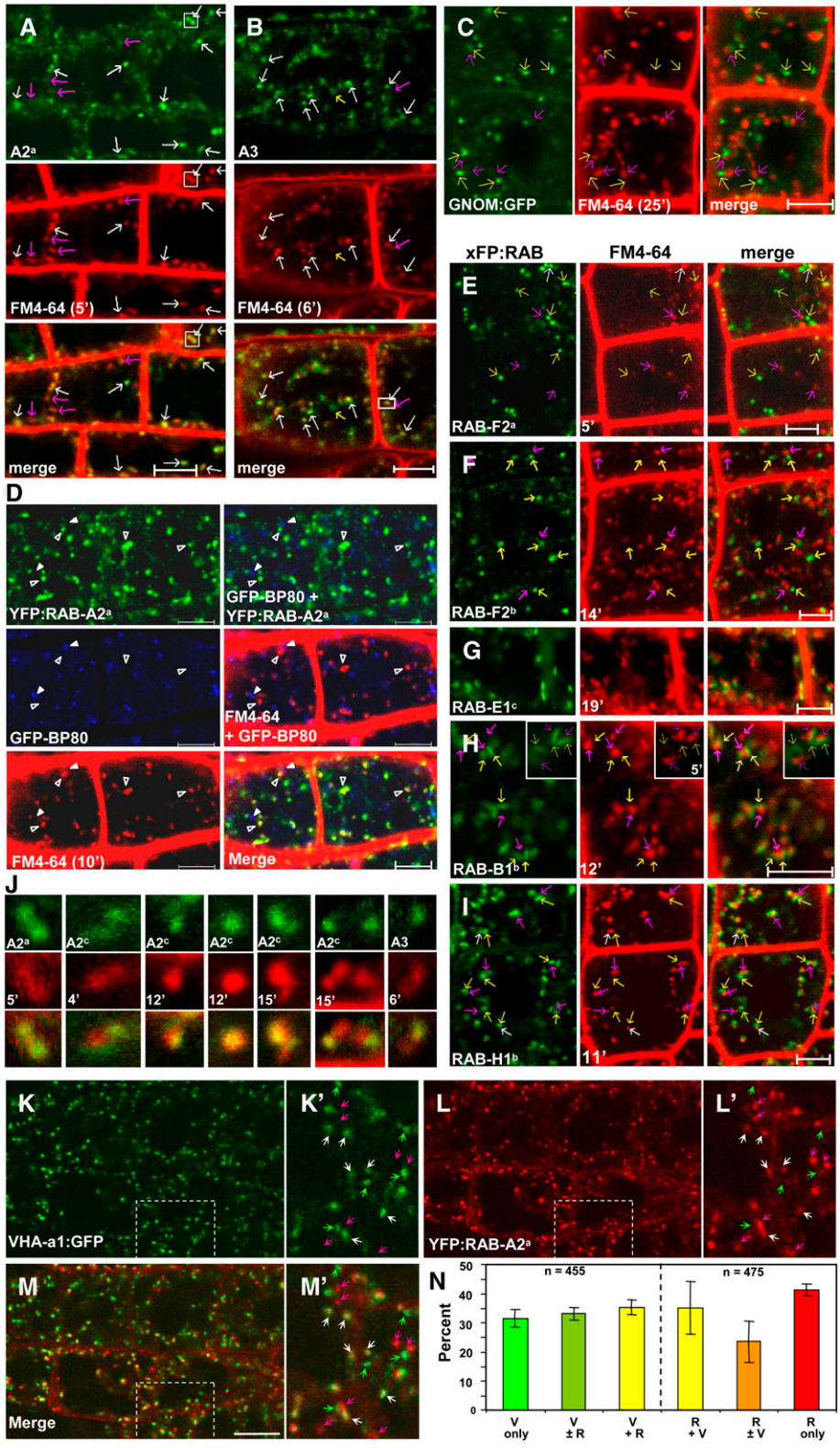

Figure 2. The Rab-A2/A3 Compartment Is Rapidly Labeled by FM4-64 and Overlaps the VHA-a1 TGN.

CLSM analysis of epidermal cells in seedling root tips. Bars = 5 μm
(A) to **(C)** and **(E)** to **(I)** Roots expressing YFP:RAB-A2[a] **(A)**, YFP:RAB-A3 **(B)**, GNOM:GFP **(C)**, YFP:RAB-F2[a] **(E)**, mRFP:RAB-F2[b] **(F)**, YFP:RAB-E1[c] **(G)**,

Rab-A2^a compartments apparently lacked the other marker. The remaining compartments exhibited weak or partial colocalization with the second marker (Figure 2N; V ± R and R ± V). Thus, the Rab-A2/A3 compartment defines a new endosomal membrane distribution that overlaps with the VHA-a1 *trans*-Golgi compartment.

The endosomes in *Arabidopsis* root tips are the primary target of the drug brefeldin A (BFA). This inhibitor causes endocytosed proteins, FM4-64, and endosomal markers such as GNOM and VHA-a1 to accumulate in large heterogeneous aggregations of membranes referred to as BFA bodies (Steinmann et al., 1999; Geldner et al., 2003; Grebe et al., 2003; Dettmer et al., 2006). By contrast, Golgi stacks and *trans*-Golgi markers such as N-ST-YFP cluster at the periphery of the BFA bodies. Supplemental Figures 10A to 10L online show that the Rab-A2/A3 compartment was rapidly affected by BFA. Rab-A2/A3 membranes accumulated at the core of the BFA compartment surrounded by membranes enriched in VHA-a1:GFP and endocytosed FM4-64, and these were in turn surrounded by Golgi and PVC markers (see Supplemental Figures 11D to 11H and 11K to 11P online). This behavior was not observed with YFP fusions to Golgi-localized Rab proteins (see Supplemental Figures 11A to 11C). One target of BFA in the *Arabidopsis* root is GNOM, but Rab-A2/A3 markers accumulated in the BFA bodies even in the presence of a BFA-resistant GNOM mutant that is sufficient for recycling PIN1 to the PM in the presence of BFA (Geldner et al., 2003) (see Supplemental Figures 10M to 10Q online). Thus, GNOM activity is not sufficient to keep Rab-A2/A3 membranes from accumulating in the BFA body.

RAB-A2 and -A3 Subclasses Relocate to the Cell Plate

In some of the meristematic cells of the root tip and young leaves, YFP:RAB-A2 and YFP:RAB-A3 proteins were seen to label single large discs or rings that resembled cell plates (Figures 3A to 3C and 3E; see Supplemental Figures 12A to 12H online). These structures were less commonly observed with YFP:RAB-A3, owing perhaps to its restricted epidermal expression domain (see Supplemental Figure 2 online). GFP:PsRAB-A3, which was expressed from the cauliflower mosaic virus (CaMV) 35S promoter, labeled similar structures throughout the meristem (Figure 3D; see Supplemental Figures 12I, 13C, 13F, 13G, and 15D online). These structures were rapidly labeled with the dye FM4-64, which is known to accumulate in the growing cell plate (Figures 3E and 3F; see Supplemental Figure 12J online). In young cell plates, YFP:RAB-A proteins were coextensive with FM4-64, but as the disc expanded, the Rab fusions were increasingly restricted to the growing margins (Figures 3E and 3F, arrows). In some cells, the cell plate appeared to adopt a bilateral symmetry, with the YFP:RAB-A protein restricted to opposite poles (Figure 3F).

Indirect immunofluorescence with anti-tubulin antibodies in root tips revealed that YFP:RAB-A2^a or -A2^d localized precisely between the opposing halves of the phragmoplast in dividing cells (Figure 3G; see Supplemental Figures 13A and 13B online). This was true at early stages, when the phragmoplast was continuous, and also later, when the expanding phragmoplast formed a ring at the growing margin of the cell plate (see Supplemental Figures 13A and 13B online). The best characterized component of membrane trafficking to the cell plate in plants is the cytokinesis-specific syntaxin KN (At SYP111). This protein appears during late prophase, when it accumulates in punctate structures, before relocating to the cell plate during cytokinesis, where it plays an essential role in vesicle fusion (Lauber et al., 1997). YFP:RAB-A2 proteins colocalized with KN at the cell plate from the earliest stages of cytokinesis to maturity (Figures 3H to 3J; see Supplemental Figures 13D and 13E online). They also colocalized substantially with KN-labeled punctate structures (white arrows in Figures 3H to 3J; see Supplemental Figures 13D and 13E online). YFP:RAB-A fusions were sometimes enriched on the cell plate relative to KN at early stages (Figure 3H) and were more distinctly peripheral on the cell plate at later stages (Figure 3J).

Analysis of wild-type root tip cells by indirect immunofluorescence at various stages of the cell cycle from preprophase to late cytokinesis confirmed that endogenous RAB-A2^a accumulated at the division plane at telophase, initially forming a disc between the phragmoplast microtubules before becoming a ring that remained precisely associated with the expanding annular phragmoplast (Figure 3K). Thus, endogenous RAB-A2^a protein accumulates at the cell plate, confirming the data obtained with the YFP:RAB-A2^a fusion.

Figure 2. (continued).

YFP:RAB-B1^b **(H)**, or YFP:RAB-H1^b **(I)** (each green) incubated with FM4-64 (red) for the times indicated. Yellow arrows indicate xFP-labeled regions without detectable FM4-64 labeling; pink arrows indicate FM4-64–labeled regions without detectable xFP signal; white arrows indicate regions with extensive overlap of xFP and FM4-64 signals. Enlarged images of the boxed areas in **(A)** and **(B)** are presented in the first and last columns in **(J)**.

(D) Seedlings coexpressing YFP:RAB-A2^a (green) and GFP-BP80 (blue) incubated with FM4-64 (red) for 10 min. YFP:RAB-A2^a– but not GFP-BP80–labeled compartments are extensively colabeled with FM4-64. Left column, single channels; right column, overlay of two or three channels as indicated. Open arrowheads indicate YFP:RAB-A2^a; arrowheads indicate GFP-BP80.

(J) Examples of punctate structures with different degrees of overlap between FM4-64 and YFP:RAB-A2/A3. Green indicates YFP fusions to members of *Arabidopsis* Rab-A2 or Rab-A3 subclasses as indicated; red indicates FM4-64 with incubation times shown.

(K) to **(M)** Seedlings coexpressing VHA-a1:GFP (green) and YFP:AtRAB-A2^a (red). K′ to M′ show enlarged areas boxed in **(K)** to **(M)**. Pink or green arrowheads indicate structures labeled only by YFP:RAB-A2^a or VHA-a1:GFP, respectively; white arrowheads indicate structures with both signals in various ratios.

(N) Quantitative assessment of the number of colocalizing VHA-a1 and Rab-A2/A3 compartments. V, VHA-a1:GFP; R, Rab-A2/A3. A total of 455 VHA-a1 compartments in images such as those in **(M)** were assigned to three categories designated V only, V ± R, and V + R, indicating that they had either no, weak, or similar intensity YFP:RAB-A2^a signals, respectively. The reciprocal analysis was done on 475 YFP:RAB-A2^a–labeled compartments, and the percentage in each category is shown. Error bars indicate SD values for data from three images.

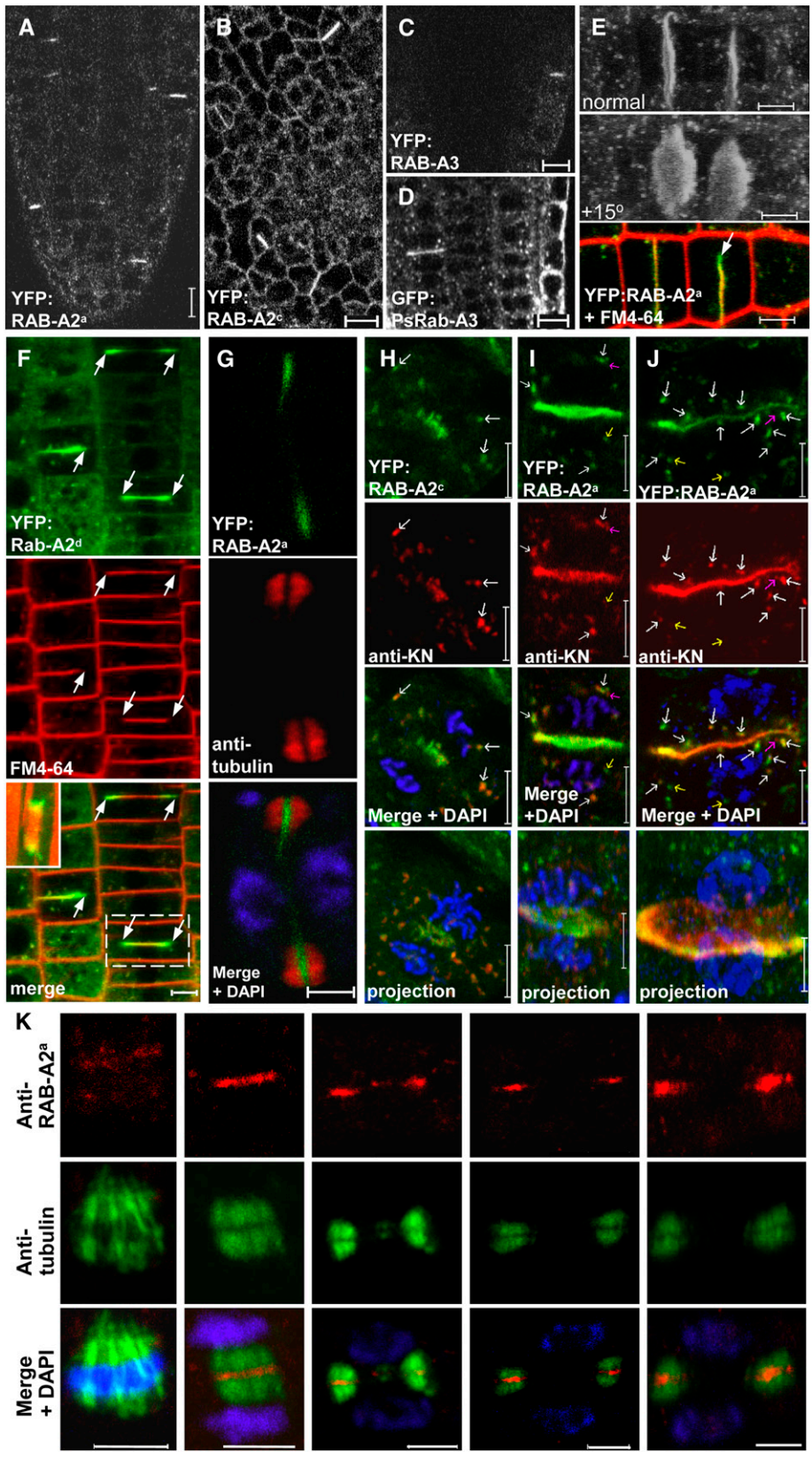

Figure 3. RAB-A2/A3 Proteins Localize to Cell Plates.

To follow the behavior of YFP:RAB-A2 and -A3 proteins over time, we performed four-dimensional image analysis (*x*, *y*, and *z* over time) of young lateral roots (see Supplemental Figure 14 and Supplemental Movie 1 online). Together, these time series revealed that Rab-A2/A3 membranes aggregate into a central disc over ~3 min, that ~15 min was required for cell plate expansion to its full extent, and that a further 15 min was then required for the dissipation of YFP:RAB-A proteins from the cell plate.

KN Accumulates in YFP:RAB-A Compartments before and during Cytokinesis

Recent work has provided evidence that KN accumulates in a multivesicular PVC prior to cytokinesis and that this compartment contributes significant membrane and wall material to the cell plate (Dhonukshe et al., 2006). As we had found that during cytokinesis KN colocalized well with YFP:RAB-A2 and -A3, which are distinct from the PVC (Figures 2D to 2F), we investigated the distribution of these markers in early stages of mitosis.

Cells at the correct stage were identified by the presence of condensed chromosomes and KN protein in dispersed punctate structures. As shown in Supplemental Figure 15A, in prophase or earlier, punctate structures that were decorated by anti-KN antibodies were partially labeled with YFP:RAB-A2 proteins. In metaphase or anaphase, however, the colocalization was precise (Figure 4A; see Supplemental Figures 15B and 15C online). By contrast, KN-positive structures at these stages were almost completely distinct from Golgi stacks (labeled with Nag:EGFP), which accumulated close by (Figure 4B). An intermediate result was obtained with GFP-BP80, which partially overlapped neighboring KN-positive structures but rarely colocalized precisely (Figure 4C).

To further clarify the identity of the KN-positive structures and the molecular composition of the cell plate, we next asked whether other markers of Golgi-associated and endosomal compartments also relocated to the division plane and whether the Rab-A2/A3 compartment retained its interphase labeling characteristics during cytokinesis. Figures 4D to 4M and Supplemental Figures 16A and 16B online show a variety of marker combinations at various stages of cytokinesis. In summary, we found no evidence for the relocation of Golgi markers (Figures 4D and 4E), PVC markers (Figures 4F to 4H; see Supplemental Figures 16A and 16B online), or GNOM (Figures 4J to 4L) to the cell plate at any stage of cytokinesis. Notably too, VHA-a1, which overlaps the Rab-A2/A3 compartment in interphase, was also excluded from the cell plate (Figure 4M), as reported previously (Dettmer et al., 2006), further highlighting the distinction between these two overlapping *trans*-Golgi compartments. Furthermore, the Rab-A2/A3 compartment appeared to retain the same characteristics in cytokinesis as in interphase. Thus, it remained close to but distinct from the Golgi stacks and PVC, as did the KN-containing punctate structures (Figures 4D to 4G), and continued to label efficiently with FM4-64 (Figure 4I; see Supplemental Figures 16C to 16E online), which was still excluded from the PVC and GNOM compartments (Figures 4H and 4J to 4L; see Supplemental Figures 16A and 16B online). Finally the YFP:RAB-A2 signal on punctate structures continued to show partial overlap with the VHA-a1 compartment in dividing cells (Figure 4M).

Relocation to the Cell Plate Is Specific for a Subset of Rab GTPase Subclasses

As YFP:RAB-A2 and -A3 fusions all relocated to the cell plate during cell division but RAB-F2 fusions did not, we asked whether the cell plate is labeled by YFP fusions to members of four other Rab subclasses, Rab-B, Rab-C1, Rab-E, and Rab-H, that have been localized to the Golgi (Cheung et al., 2002; Kotzer et al., 2004; Lee et al., 2004; Zheng et al., 2005; C.M. Chow, S. Rutherford, and I. Moore, unpublished data). To identify dividing cells, we either introduced GFP:PsRAB-A3, which quantitatively colocalizes to the cell plate along with YFP:RAB-A2 and -A3 proteins (see Supplemental Figure 17A online), or used immunofluorescence with KN antibodies. All dividing cells expressing GFP:PsRAB-A3 exhibited GFP signals at the cell plate that were

Figure 3. (continued).

CLSM analysis of seedlings.

(A) to **(F)** RAB-A2/A3 targeted xFP to cell plate–like structures, which were rapidly labeled with FM4-64. Meristemic tissues of root tips (**[A]** and **[C]** to **[F]**) or young true leaves **(B)** of *Arabidopsis* seedlings expressing fluorescent protein fusions to At RAB-A2^a (**[A]** and **[E]**), At RAB-A2^c **(B)**, At RAB-A2^d **(F)**, At RAB-A3 **(C)**, or Ps RAB-A3 **(D)**. xFP:RAB-A is shown in white or green; FM4-64 is shown in red. xFP:RAB signals were seen to concentrate in linear structures in single optical sections (**[A]** to **[D]**; bars = 10 μm).

(E) Top two panels, three-dimensional reconstruction at two different angles from serial optical sections of YFP:AtRAB-A2^a–labeled discs; bottom panel, single optical section showing that these structures label with FM4-64 (red) but with a higher relative abundance of YFP:AtRAB-A2^a at the periphery of the incomplete disc (arrow). Bars = 5 μm.

(F) YFP:AtRAB-A2^d (green) is concentrated at the periphery (arrows) of FM4-64 (red)–labeled cell plates. The three-dimensional reconstruction from serial sections of the dotted area is shown as an inset. Note that some of the YFP- and FM4-64–labeled cell plates have open ends. Bar = 5 μm.

(G) to **(J)** Immunolocalization of α-tubulin **(G)** or KN (**[H]** to **[J]**) in meristemic tissues of root tips of 5-d-old *Arabidopsis* seedlings expressing YFP:AtRAB-A2^a (**[G]**, **[I]**, and **[J]**) or YFP:AtRAB-A2^c **(H)**. Microtubules or KN are shown in red; DAPI is shown in blue; YFP is shown in green. White arrows indicate extensive overlap between YFP:AtRAB-A and KN signals; yellow arrows indicate YFP:AtRAB-A signal alone; pink arrows indicate KN signal alone. In **(H)** to **(J)**, three-dimensional reconstruction images of serial optical sections are shown as merged images below the single optical sections in the top three rows. Bars = 5 μm.

(K) Endogenous At RAB-A2^a localizes to the cell plate. Double immunolocalization of α-tubulin (green) and RAB-A2^a (red) in wild-type root tips of 5-d-old *Arabidopsis* seedlings stained with DAPI (blue). Affinity-purified anti-RAB-A2^a (1:3000) was used to probe the native Rab-A2^a proteins at different stages of mitosis and cytokinesis, including metaphase and telophase. Note that RAB-A2^a only concentrated in the midzone of microtubule arrays in telophase. First to fourth columns, single section images; fifth column, three-dimensional reconstruction from serial images along the *z* axis. Bars = 5 μm.

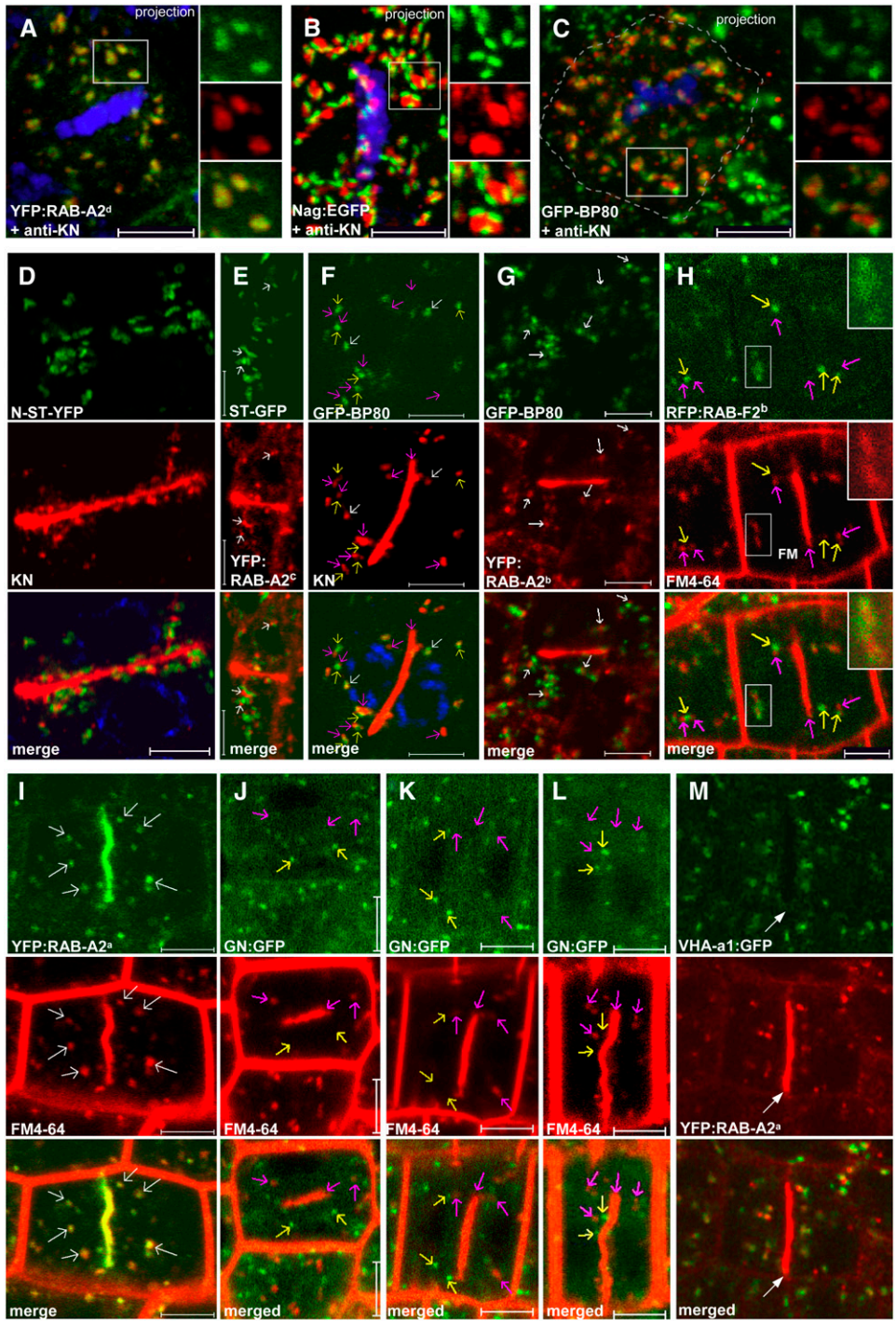

Figure 4. Rab-A2/A3 Membranes Colocalize with KN in Mitosis and Maintain Their Identity during Cytokinesis.

CSLM analysis of mitotic and dividing root tip cells expressing various Golgi and endosomal or prevacuolar markers. Three-dimensional reconstruction images are shown in **(A)** to **(C)**, while single section images are shown in **(D)** to **(M)**. Bars = 5 μm.

(A) to **(D)** and **(F)** Immunolocalization of KN (red) at metaphase (**[A]** to **[C]**) or telophase (**[D]** and **[F]**) in roots expressing YFP:AtRAB-A2^{d}, Nag:EGFP, GFP-BP80, or N-ST-YFP (green) stained with DAPI (blue). Enlarged images of boxed areas in **(A)** to **(C)** are shown at left of each image as single channels and merged images. The dashed line in **(C)** indicates the boundary of the mitotic cell.

(E) and **(G)** Dividing root tip cells coexpressing ST-GFP or GFP-BP80 with YFP:AtRAB-A2^{c} or -A2^{b}. White arrows indicate YFP:AtRAB-A2 proteins, which are close to ST-GFP or GFP-BP80.

(H) to **(M)** Dividing root tip cells expressing RFP:AtRAB-F2^{b}, YFP:AtRAB-A2^{a}, GNOM:GFP (GN:GFP), or VHA-a1:GFP as indicated, stained with FM4-64. In **(F)** and **(H)** to **(L)**, white arrows indicate colocalizing structures and yellow or pink arrows indicate structures that have only green or red signal, respectively. The arrow in **(M)** indicates a cell plate labeled by YFP:AtRAB-2^{a} but not VHA-a1.

either similar to or stronger than the punctate compartments in the same cell (Table 1). Tagged RAB-B1[b] or RAB-C1 were never observed on the cell plate at any stage of cytokinesis (Table 1; see Supplemental Figure 17A online). With YFP:RAB-H1[b], weak fluorescence was commonly observed on the cell plate in addition to Golgi-localized signal (see Supplemental Figures 17A and 17B online), but the intensity of the YFP:RAB-H1[b] signal on the cell plate never exceeded its intensity on the Golgi stacks in the same cell (Table 1). YFP:RAB-E1[c] (ARA3) (Anai et al., 1991; Zheng et al., 2005) labeled the cell plate less often than YFP:RAB-H1[b], but the labeling was often stronger (Table 1; see Supplemental Figures 17A and 17B online). However, none of the tagged Rab proteins that we tested relocated to the cell plate to the same extent as members of the Rab-A2 and Rab-A3 subclasses (Table 1).

GTP Binding and Hydrolysis Mutants Relocate RAB-A2[a] toward the Golgi and PM, Respectively

To investigate the function of the Rab-A2 subclass in *Arabidopsis*, we generated mutants of RAB-A2[a] that were predicted either to preferentially bind GDP and thus to stabilize the inactive state (RAB-A2[a][S26N]) or to be GTPase-deficient and thus to stabilize the GTP-bound active state (RAB-A2[a][Q71L]) (Olkkonen and Stenmark, 1997; Ueda et al., 2001; Sohn et al., 2003; Kotzer et al., 2004; Lee et al., 2004; Zheng et al., 2005). Mutations were introduced into the genomic sequence of RAB-A2[a], and the mutated sequences were exchanged for the wild-type sequence in the YFP fusion vector (see Supplemental Figure 1A online). The localization of the resulting fusions was examined in root tips of transgenic seedlings.

YFP:RAB-A2[a][S26N] showed increased cytosolic labeling relative to the wild type but also labeled punctate structures that colocalized more extensively than wild-type YFP:RAB-A2[a] with a Golgi marker (Figure 5A). The degree of colocalization was higher in transgenic lines with higher expression levels, and the colocalization with FM4-64 was correspondingly reduced (Figure 5B). Upon BFA treatment, YFP:RAB-A2[a][S26N] relocated less extensively than the wild type to the BFA bodies, consistent with an increased Golgi localization (Figure 5C). Like YFP:RAB-A2[a][S26N], YFP:RAB-A2[a][Q71L] also showed increased cytosolic labeling relative to the wild type; by contrast, it was targeted predominantly to the cell periphery rather than to punctate organelles (Figure 5A). Upon BFA treatment, however, some YFP:RAB-A2[a][Q71L] colocalized with FM4-64 in the BFA body, although labeling at the periphery was maintained (Figure 5C). Finally, both fusions were observed on the cell plate in dividing cells (Figure 5D) and were preferentially concentrated at the growing margins at later stages of cytokinesis. These results suggested that RAB-A2[a] associates with organelles on a pathway from the Golgi to the PM in interphase and that in dividing cells the GDP-bound and GTP-bound forms both act at the cell plate.

Table 1. Intensity of Cell Plate Labeling by GFP:PsRAB-A3 and YFP Fusions to Various *Arabidopsis* Rab GTPase Subclasses

Category	GFP: PsRAB-A3	YFP: RAB-B1[b]	YFP: RAB-C1	YFP: RAB-H1[b]	YFP: RAB-E1[c]
No CP	0	100	100	20	32
CP < P	0	0	0	55	14
CP = P	15	0	0	25	37
CP > P	85	0	0	0	17
Total CP[a]	55	32	18	20	35
Total roots[b]	27	11	14	11	16

Values shown are percentages of cell plates. CP, cell plate; P, punctate compartments; No, <, =, and > indicate that labeling of the CP was either absent or less than, similar to, or more than the labeling of the punctate compartment, respectively.
[a] Total number of cell plates analyzed.
[b] Number of root tips that were analyzed.

Dominant-Inhibitory Mutants of RAB-A2[a] Inhibit Cytokinesis

To investigate the requirement for RAB-A2[a] function in cytokinesis, we expressed untagged wild type and S26N and Q71L mutants in transgenic plants using the pOp6/LhGR-inducible promoter system (Craft et al., 2005). The S26N and Q71L mutants were expected to act as dominant-inhibitory and dominant gain-of-function alleles, respectively (Olkkonen and Stenmark, 1997). In addition, another dominant-inhibitory mutant, N125I, was also expressed. This substitution, equivalent to N116I of Ras, reduces the affinity of small GTPases for nucleotides (Olkkonen and Stenmark, 1997), thereby promoting the nucleotide-free state and generating a strong dominant-inhibitory protein (Schmitt et al., 1986; Jones et al., 1995; Olkkonen and Stenmark, 1997; Batoko et al., 2000; Zheng et al., 2005). When expressed as a YFP fusion, YFP:RAB-A2[a][N125I] accumulated to lower levels than wild-type YFP:RAB-A2[a], consistent with the relative instability of the nucleotide-free form (Olkkonen and Stenmark, 1997), but was targeted like the wild type to BFA-sensitive punctate structures that labeled with FM4-64 (see Supplemental Figure 18 online). For dexamethasone-inducible expression, wild-type and mutant sequences were cloned in pH-TOP and introduced into the homozygous driver line 4C-S5/7, which expresses the dexamethasone-inducible transcription factor LhGR from the CaMV 35S promoter (Craft et al., 2005).

T2 populations were germinated on medium with or without dexamethasone. In all 53 lines obtained with the wild-type RAB-A2[a] construct, seedlings developed normally on both media, but 27 of the 47 S26N lines, 14 of the 44 Q71L lines, and 19 of the 28 N125I lines segregated seedlings with strongly inhibited growth on dexamethasone-containing medium (Figure 6A). Induced phenotypes were strongest for N125I lines and least severe in the Q71L lines. Induced expression from the CaMV 35S LhGR driver line 4C-S5/7 used in these experiments was significantly weaker in the root meristem than in the elongation zone and mature tissues (see Supplemental Figure 19 online), but in the most severely affected lines the induced phenotypes extended into the meristem. In these lines, RAB-A2[a][N125I] caused severely abnormal cell expansion and disrupted the normally regular cell files (Figure 6B). Similar but weaker phenotypes appeared in S26N and Q71L lines, particularly after longer exposure to dexamethasone, but they were not observed in lines expressing wild-type RAB-A2[a] (Figure 6B). When such root

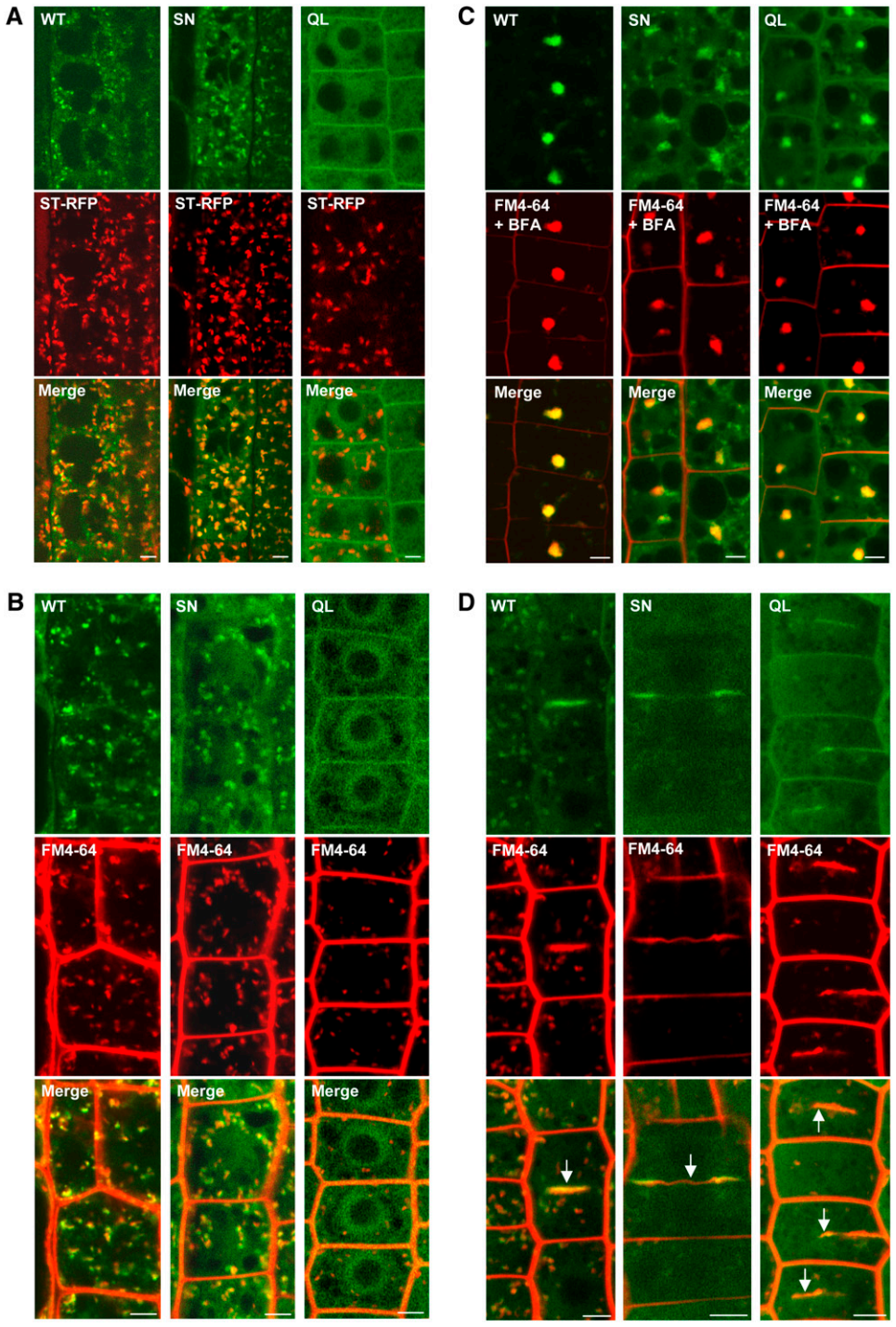

Figure 5. Localization of Mutant At RAB-A2^a Proteins.

YFP-tagged At RAB-A2^a wild type (WT), S26N (SN) mutant, or Q71L (QL) mutant (each green) with either the Golgi marker ST-RFP or FM4-64 (each red) as indicated. **(C)** shows cells after treatment with BFA. **(D)** shows dividing cells with labeled cell plates (arrows in merged images). All images are confocal sections of seedling root tips. Bars = 4 μm.

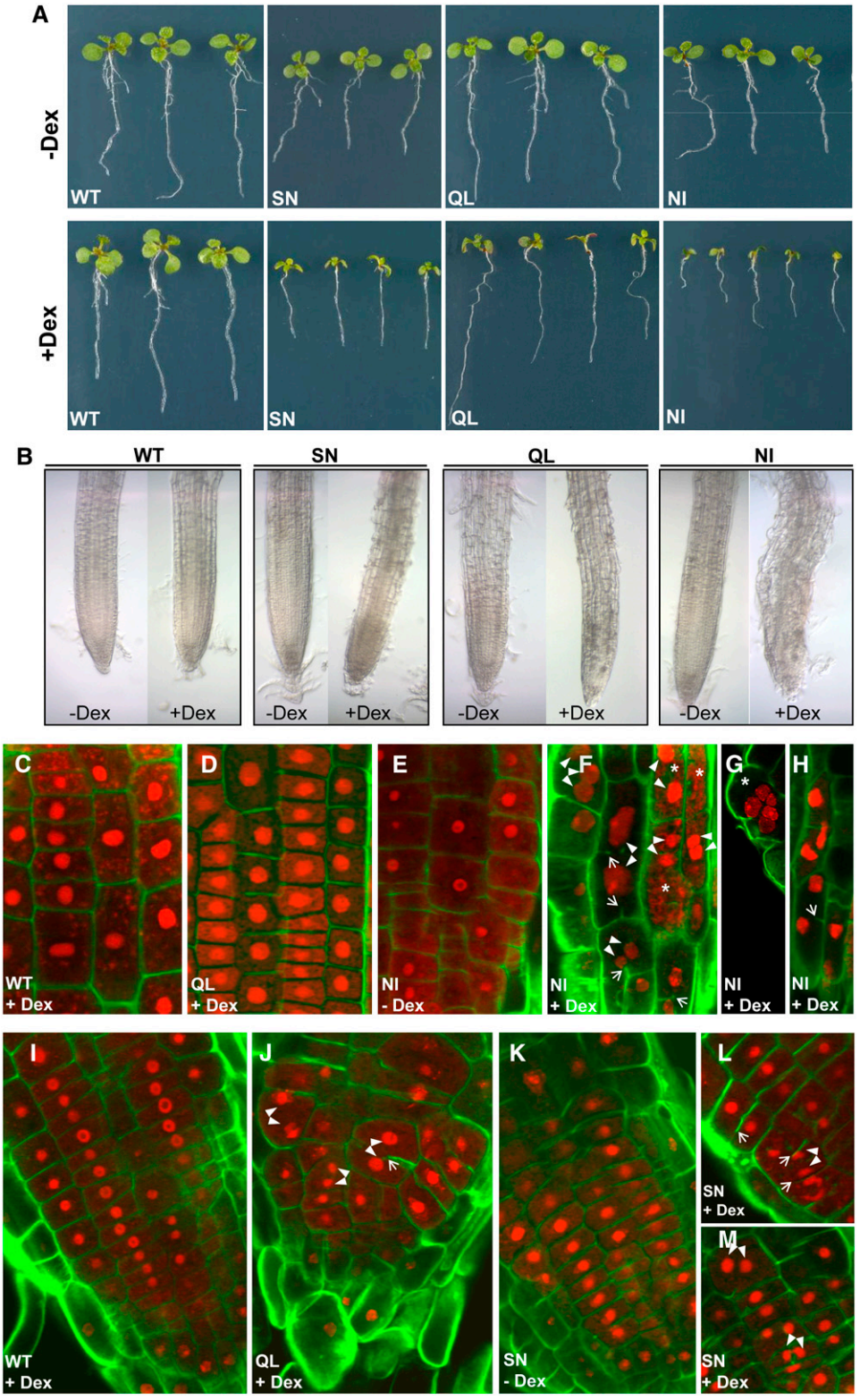

Figure 6. Dominant-Inhibitory At RAB-A2^a Mutants Block Cytokinesis.

At RAB-A2^a wild type and S26N (SN), Q71L (QL), or N125I (NI) mutants were expressed in seedlings from a dexamethasone-inducible promoter.
(A) and **(B)** Eleven-day-old seedlings **(A)** and their primary root tips **(B)** germinated and grown in the presence of 20 μM dexamethasone (+Dex) or the equivalent quantity of DMSO solvent (−Dex).
(C) to **(M)** Confocal images of propidium iodide–stained nuclei (red) and Calcofluor-stained cell walls (green) in 7-d-old seedlings (**[C]** to **[H]**) or 14-d-old seedlings (**[I]** to **[M]**) grown with (+Dex) or without (−Dex) dexamethasone. Arrowheads in **(F)**, **(J)**, **(L)**, and **(M)** indicate multiple nuclei in single cells; arrows indicate cell wall stubs. Serial confocal sections of the cells marked by asterisks in **(F)** and **(G)** revealed that they had four and six nuclei, respectively.

tips were stained for cell walls and nuclei, the epidermal cells of N125I lines exhibited a high incidence of binucleate cells (Figures 6C to 6H). In addition, highly irregular cell files, cell wall stubs, and incomplete cell walls could be observed in these seedlings (Figures 6F to 6H). Serial confocal sections revealed that the large and irregularly swollen cells were multinucleate (Figure 6G). Therefore, it appears that these cells had undergone successive rounds of mitosis and nuclear division without completing cytokinesis. In lines expressing S26N, the swollen epidermal cells were also multinucleate, although such cells were observed less commonly and appeared later after germination (Figures 6K to 6M). By contrast, cell files and cytokinesis were apparently normal in lines expressing wild-type RAB-A2^a (Figures 6C and 6I) and were rarely perturbed in Q71L lines (Figure 6J), despite their abnormal development (Figure 6A).

In summary, the phenotypes of plants expressing dominant-inhibitory mutants of RAB-A2^a indicated that RAB-A2^a interacts with a factor that is essential for cell plate formation, consistent with its localization at the margins of the cell plate.

DISCUSSION

The Rab-A2/A3 Compartment in *Arabidopsis* as a Domain of the TGN

We show here that two subclasses within the large Rab-A group, Rab-A2 and Rab-A3, identify a distinct early endosomal TGN-associated membrane domain, which we have named the Rab-A2/A3 compartment. Targeting appears to be conserved among plant Rab-A3 proteins, as GFP:PsRAB-A3 (PRA2 of pea) (Inaba et al., 2002) colocalized with YFP:RAB-A3. The ability to target YFP to this compartment was specific for members of the Rab-A2 and Rab-A3 subclasses, as fusions to members of the Rab-B, Rab-C1, Rab-E, or Rab-F2 subclasses were each targeted to the Golgi or PVC.

The Rab-A2/A3 compartment often lay in close proximity to the Golgi stacks and the PVC labeled by GFP-BP80, although it was distinct from both and could be found isolated from either structure. Approximately 70% of Rab-A2/A3 compartments are labeled at least partially by a TGN marker, the VHA-a1 subunit of the V-ATPase (Dettmer et al., 2006). The close association of Golgi, multivesicular bodies (MVBs), and a TGN-like compartment was also shown recently by electron tomography (Segui-Simarro and Staehelin, 2006). The MVBs in that study probably include the PVC that is labeled by vacuolar sorting receptors such as BP80 (Tse et al., 2004).

The VHA-a1 compartment is considered a putative TGN, as it lies on the endocytic and biosynthetic pathways (Dettmer et al., 2006). The Rab-A2/A3 compartment apparently also resides on the endocytic and biosynthetic pathways (see below). VHA-a1 and RAB-A2/A3 nevertheless exhibit distinct distributions, as the two markers often failed to colocalize precisely on the same structure and approximately one-third of the VHA-a1 and Rab-A2/A3 compartments lacked the other marker. Furthermore, in dividing cells, YFP:RAB-A2/A3 redistributed to the cell plate but VHA-a1 did not. VHA-a1 and RAB-A2 or -A3 proteins may reside on distinct compartments that are often in close association and therefore unresolved by light microscopy. Alternatively, they may reside on subdomains of the same compartment that either gives rise to or are derived from compartments that carry only VHA-a1 or RAB-A2 and -A3 proteins. Consistent with this, Rab-A2/A3 compartments were not uniformly labeled by FM4-64, and individual FM4-64–positive endosomes were often incompletely decorated with Rab-A2/A3 markers. In addition, membrane labeled only by FM4-64 could be seen to separate from colocalizing regions and may be enriched in VHA-a1. To date, we have not been able to obtain clear simultaneous resolution of VHA-a1:GFP, YFP:RAB-A2, and FM4-64 to test this hypothesis. Nevertheless, the results of this study show that the TGN/EE system is more complex than simply involving the VHA-a1 compartment in *Arabidopsis* root tips. They also show that this compartment can reside at a considerable distance from the Golgi and only temporarily lie in close proximity to it.

The Rab-A2/A3 Compartment as an Early Endosomal Compartment

In *Arabidopsis* root tips, endosomal compartments have been characterized by early labeling with FM4-64, whose uptake is clathrin-dependent (Geldner et al., 2003; Bolte et al., 2004; Russinovaa et al., 2004; Takano et al., 2005; Dettmer et al., 2006; Dhonukshe et al., 2007). Like the VHA-a1 TGN (Dettmer et al., 2006), the Rab-A2/A3 compartment is an early site of FM4-64 labeling. FM4-64 may act as a tracer of the endocytic pathway, as it progressively and selectively labels compartments over a period of 2 h, starting with the PM and ending with the tonoplast (Dettmer et al., 2006). Furthermore, its transport to the tonoplast can be disrupted in various systems by mutant proteins or drugs that are proposed to act on some aspect of membrane trafficking (Bloch et al., 2005; Yamada et al., 2005; Dettmer et al., 2006; Dhonukshe et al., 2006). Triple labeling experiments showed that FM4-64 accumulates in the Rab-A2/A3 compartment significantly before it is seen in the PVC, which is identified by vacuolar sorting receptors such as GFP-BP80 and the Rab-F2 subclass (Kotzer et al., 2004; Lee et al., 2004). This is consistent with the findings of Dettmer et al. (2006) but is at odds with the proposal that the Rab-F2 compartment is an EE and early site of FM4-64 accumulation (Ueda et al., 2004). These differences may be attributable to the use of a protoplast system rather than transgenic root tips.

In *Arabidopsis* root tips, endosomal compartments accumulate within BFA bodies in the presence of BFA (Steinmann et al., 1999; Friml et al., 2002; Grebe et al., 2002, 2003; Geldner, 2004; Teh and Moore, 2007). YFP-tagged Rab-A2 and Rab-A3 proteins colocalized precisely with FM4-64 and the recycling PM protein PIN1 in the BFA bodies. By contrast, several markers of a prevacuolar MVB (GFP-BP80, YFP:RAB-F2^a, and mRFP1:RAB-F2^b) (Kotzer et al., 2004; Preuss et al., 2004; Ueda et al., 2004; Takano et al., 2005) were largely excluded from the BFA body, suggesting that these membranes do not contribute substantially to it.

When FM4-64 was added to cells pretreated with BFA, FM4-64 accumulated first at the periphery of the BFA body in a region enriched in VHA-a1 relative to RAB-A2/A3 proteins. Therefore, TGN/EE domains enriched in VHA-a1 may be the first site of

FM4-64 accumulation. These studies also revealed unsuspected structure in the BFA body: a core enriched in Rab-A2/A3 membranes, which responded most rapidly to BFA, is surrounded first by membrane enriched in VHA-a1 and subsequently by Golgi stacks and PVC.

The Rab-A2/A3 Compartment Apparently Lies on a Secretory Pathway

Evidence placing the VHA-a1 TGN/EE compartment on the exocytic pathway is currently limited and indirect. It is based on the cycloheximide-sensitive accumulation of a recycling membrane protein marker in the VHA-a1 compartment in the presence of the V-ATPase inhibitor concanamycin-A (Dettmer et al., 2006). Analysis of GTP binding and hydrolysis mutants of RAB-A2^a provides additional independent evidence that the Rab-A2/A3 domain lies on a pathway from the Golgi to the PM.

First, the RAB-A2^a[S26N] mutant that is predicted to favor GDP binding relocated toward the Golgi from the Rab-A2/A3 compartment. Rab GTPases are recruited from the cytosol in the GDP-bound form and are subsequently converted to the GTP-bound form by guanine-nucleotide exchange factors (GEFs) (Olkkonen and Stenmark, 1997). By promoting GDP binding over GTP binding, the S26N mutation can titrate and inhibit interactors of the GDP-bound state such as membrane receptors and GEFs (Olkkonen and Stenmark, 1997; Sohn et al., 2003; Kotzer et al., 2004; Lee et al., 2004), and this may account for its prolonged retention at the Golgi. Indeed, redistribution to the Golgi was increasingly pronounced as expression levels increased. Therefore, we suggest that GDP-bound RAB-A2^a is normally recruited to the Golgi and rapidly trafficked to the Rab-A2/A3 compartment following conversion to the GTP-bound form.

Second, the Q71L form of the protein that is predicted to be GTPase-deficient resided at the PM, placing the Rab-A2/A3 compartment on a secretory pathway. We do not know whether the GTP-bound form of the protein normally functions at the PM, where a small quantity of wild-type protein is located, or whether the mutant protein is carried there only as a result of slow GTP hydrolysis, which is a prerequisite for recycling off the membrane (Olkkonen and Stenmark, 1997). Nevertheless, these observations place RAB-A2^a and the Rab-A2/A3 compartment on a secretory pathway rather than a vacuolar pathway from the Golgi.

Consistent with this is the observation that the Rab-A2/A3 compartment accumulates newly synthesized KN protein and that dominant-inhibitory mutants in RAB-A2^a inhibit the formation of the cell plate, which is a major destination for biosynthetic cargo in dividing cells (Jürgens, 2005).

A Model for the Endosomal System in the *Arabidopsis* Root Tip

Figure 7A presents a model of the *Arabidopsis* endosomal system incorporating the observations from this study. Central is the TGN/EE, which is shown here to have two domains: a VHA-a1–enriched domain, which may be the earliest destination for FM4-64, and the Rab-A2/A3 domain, which lies on the biosynthetic route from the Golgi to the PM. As the Rab-A2/A3 domain lies on the exocytic route to the PM, it may provide a rapid recycling route. Such a pathway could account for the slow rate at which FM4-64 moves from the Rab-A2/A3 TGN/EE domain (labeled within 5 min) to the later endosomes, PVC, and tonoplast, which requires ~2 h.

The PVC compartment on which vacuolar sorting receptors and Rab-F2 proteins reside (Kotzer et al., 2004; Lee et al., 2004; Haas et al., 2007) is labeled slowly with FM4-64 and is largely insensitive to BFA, so it is placed downstream of the TGN/EE. Consistent with this, the Rab-F2/BP80 compartment has been identified in tobacco and *Arabidopsis* as an MVB (Tse et al., 2004; Otegui et al., 2006; Haas et al., 2007), which has been considered a later station on the endocytic route in plant cells (Tanchak et al., 1988; Geldner, 2004; Lam et al., 2007b) and other eukaryotes (Marcote et al., 2000; Pelham, 2002; Prescianotto-Baschong and Riezman, 2002; Geldner, 2004; Gruenberg and Stenmark, 2004). The Rab-F2 subclass is also involved in sorting vacuolar cargo from the Golgi, while the Rab-F2 compartment accumulates vacuolar sorting receptors and vacuolar GFP markers en route to the vacuole (Sohn et al., 2003; Kotzer et al., 2004; Zheng et al., 2005; Samalova et al., 2006), so the endocytic and vacuolar pathways may converge at the Rab-F2/BP80 compartment (Lam et al., 2007b). This is consistent with cytochemical data that show a convergence of endocytic and vacuolar pathways at a MVB (Record and Griffing, 1988) and also with the situation in fungal and animal cells, in which vacuolar and endocytic pathways converge at multivesicular endosomes (Pelham, 2002; Gruenberg and Stenmark, 2004). It is unclear whether sorting to the vacuole is from the TGN/EE or the Golgi stack itself in the *Arabidopsis* root tips, but in other plant systems vacuolar sorting receptors and Rab-F2 proteins distribute between the PVC and the Golgi stacks, where the GDP-bound inhibitory form of Rab-F2^b also localizes (Kotzer et al., 2004; daSilva et al., 2005, 2006).

The GNOM compartment has been positioned variously downstream or upstream of the PVC (Geldner et al., 2003; Geldner, 2004; Ueda et al., 2004; Jaillais et al., 2007) but could also reside on a separate recycling pathway from TGN/EE (Figure 7A). As shown here, it labels slowly with FM4-64 relative to the Rab-A2/A3 and VHA-a1 compartments, suggesting that it is downstream of the TGN/EE in the FM4-64 transport pathway, although independent pathways of FM4-64 transport to the TGN/EE, PVC, and GNOM compartments cannot be ruled out. Furthermore, in contrast with the PVC, GNOM relocates efficiently to the BFA body and is wortmannin-insensitive (Geldner et al., 2003; Tse et al., 2004; daSilva et al., 2006; Jaillais et al., 2006; Miao et al., 2006; Oliviusson et al., 2006) (see Supplemental Figures 11I and 11J online), suggesting that it may be associated more closely with an earlier endosomal compartment than with the later PVC.

The Endosomal System in *Arabidopsis* Root Tips, Budding Yeast, and Mammals

The model in Figure 7A places the *Arabidopsis* Rab-F2 subclass, which is similar to Rab5 of the mammalian EE, downstream of Rab-A2/A3 subclasses, which are related to Rab11 and Rab25 of the mammalian recycling endosome (Figure 7B). Thus, the relative positions of the Rab5- and Rab11-related proteins on

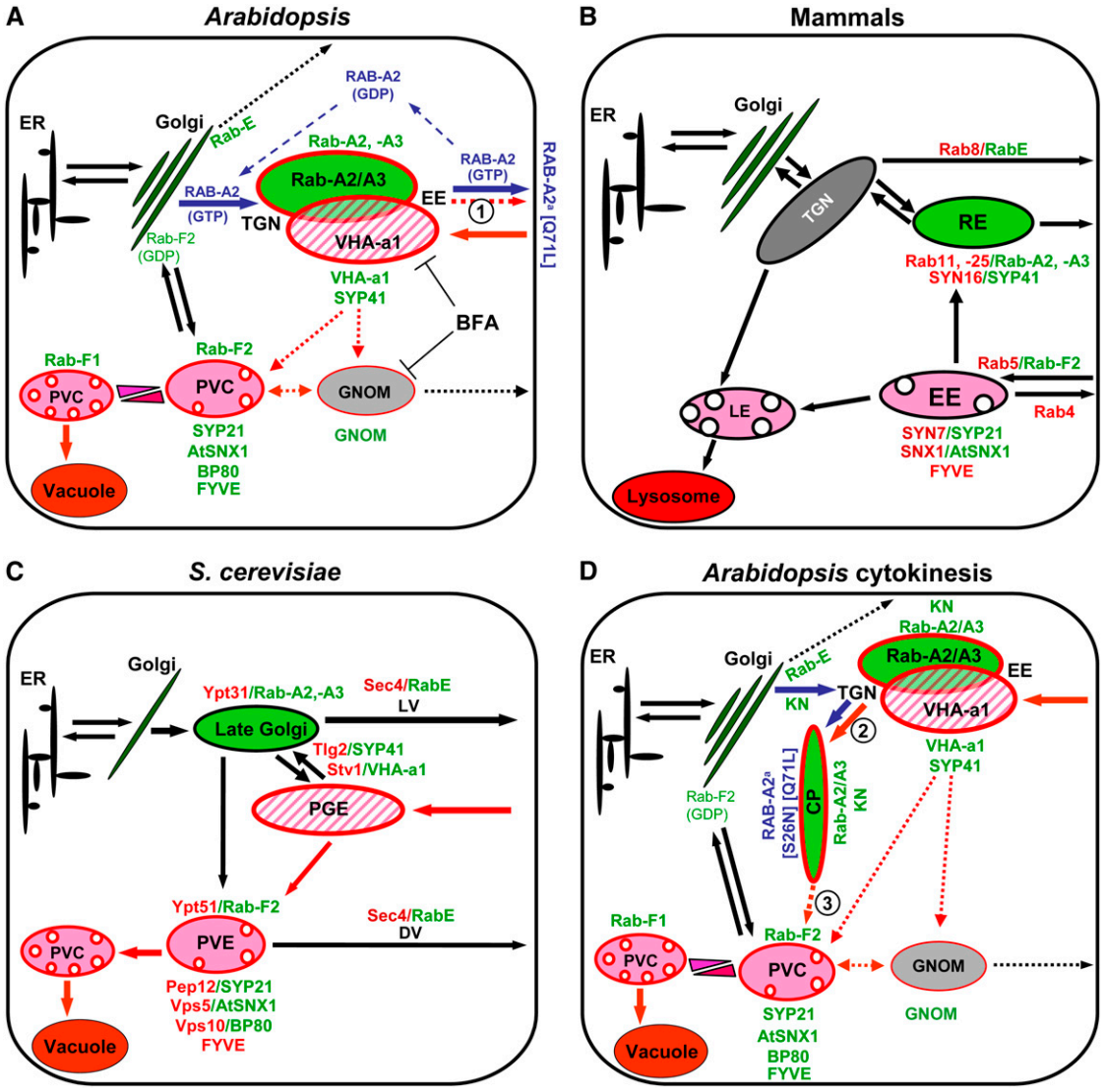

Figure 7. Schematic Models of Endosomal and Prevacuolar/Lysosomal Compartments in *Arabidopsis* Root Tips, Yeast, and a Nonpolarized Mammalian Cell.

(A) Model for the organization of the endosomal system in *Arabidopsis* root tips based on the results of this study; the Rab-A2/A3 compartment overlaps the VHA-a1 TGN compartment and is an EE on the FM4-64 uptake pathway (red arrows and compartments). The proposed pathway of At RAB-A2ª cycling is shown in blue arrows, with dashed arrows indicating cycling on and off membranes. Markers for each compartment are indicated in green. Dotted arrows are hypothetical. In accordance with Ueda et al. (2004), the Rab-F1 PVC is placed downstream of the overlapping Rab-F2 PVC, which is a multivesicular body. The position of the GNOM recycling compartment is unclear. FYVE is a PI(3)P binding marker. ER, endoplasmic reticulum. Circled numbers in all panels designate transport steps referred to in the text.

(B) and **(C)** Schematic representations of the mammalian and *S. cerevisiae* endosomal systems after Gruenberg and Stenmark (2004), Prescianotto-Baschong and Riezman (2002), and Pelham (2002). Markers of each compartment are shown in red letters, with their *Arabidopsis* homolog in green. The mammalian EE shares several markers with the *Arabidopsis* PVC and yeast prevacuolar endosome (PVE), which are both later endosomes. The *Arabidopsis* Rab-A2/A3 and VHA-a1 compartments share markers with the closely connected yeast late-Golgi and post-Golgi endosome (PGE), which is also an EE. Light (LV) and dense (DV) vesicles mediate alternative routes to the cell surface in *S. cerevisiae* (Harsay and Schekman, 2002). The orthologous Rab and SNARE proteins label the mammalian recycling endosome, which lies downstream of the EE, on the secretory pathway for many proteins.

(D) The cell plate shares markers specifically with the Rab-A2/A3 membrane domain but also apparently accumulates both GDP- and GTP-bound forms of RAB-A2ª; the position of the Rab-A2/A3 domain on the exocytic and endocytic routes can account for the appearance of endocytosed molecules such as FM4-64 in the cell plate.

the endocytic pathway would be reversed in *Arabidopsis*. We note, however, that this arrangement is similar to that in *S. cerevisiae*. There, YPT31/32, the paralogues of Rab-A2/A3, reside at the late Golgi, where they play roles in biosynthetic traffic and in recycling proteins to the TGN from the early post-Golgi endosome (Pelham, 2002; Chen et al., 2005; Ortiz and Novick, 2006). Traffic at the late Golgi and post-Golgi endosome is mediated by the Tlg SNARE complex that is paralogous to SYP41 at the *Arabidopsis* TGN/EE (Pelham, 2002; Sipos et al., 2004; Dettmer et al., 2006). Yeast also possess a paralogue of the VHA-a1 subunit, Stv1p, which resides in late Golgi membranes and appears to cycle through early and prevacuolar endosomes (Sipos et al., 2004; Kane, 2006). Furthermore, yeast Vps21/Ypt51, which is a paralogue of Rab-F2, lies on a later prevacuolar endosome that gives rise to the multivesicular PVC (MVB/PVC) (Pelham, 2002; Prescianotto-Baschong and Riezman, 2002). It has been noted that the yeast prevacuolar endosome and the mammalian EE share several other markers, including PI(3)P, Snx1/Vps5, Pep12/Syntaxin7 and 13, Rabenosyn5/Vac1, and Hrs/Vps27, and are likely to be equivalent (Pelham, 2002). Furthermore, the mammalian EE is also recognized as the compartment in which multivesicular bodies begin to form (Gruenberg and Stenmark, 2004). Thus, the *Arabidopsis* Rab-A2/A3 and VHA-a1 compartments may be homologous with the yeast TGN and post-Golgi endosome (Sipos et al., 2004; Chen et al., 2005; Kane, 2006; Ortiz and Novick, 2006), while the Rab-F2 compartment may be homologous with the prevacuolar endosome (Figures 7A and 7C).

Evidence in this study that places the Rab-A2/A3 compartment between the Golgi and the PM but also on the early endocytic pathway strengthens the similarity with the yeast late Golgi. The corresponding compartment in mammalian cells may be the recycling endosome, through which many newly synthesized proteins travel on their way to the PM (Rodman and Wandinger-Ness, 2000; Gruenberg and Stenmark, 2004). Although plant Rab-F2 proteins have been discussed in relation to EEs by analogy with mammalian Rab5 (Ueda et al., 2004; Geldner, 2004; Lam et al., 2007b), this may be a misleading comparison, and we suggest that yeast prevacuolar endosome may be more closely related to the plant Rab-F2 compartment. Nevertheless, additional roles for the Rab-F2 subclass in endocytosis cannot be ruled out, as dominant-negative RAB-F2^{b} can inhibit FM4-64 uptake into BY2 cells (Dhonukshe et al., 2006). Indeed, the functionally overlapping Ypt51/52/53 paralogues of Rab-F2 in yeast also contribute to early stages of endosomal traffic (Pelham, 2002; Prescianotto-Baschong and Riezman, 2002).

The Rab-A2/A3 Compartment Contributes Substantially to the Cell Plate

The cell plate is a novel intracellular compartment assembled by membrane traffic, but its origin is unclear (Jürgens, 2005). The only dedicated component of the trafficking pathway to the cell plate is the cytokinesis-specific syntaxin KN/SYP111, which accumulates in a Golgi-derived compartment during preprophase and mitosis and is rapidly degraded once cytokinesis is complete (Lauber et al., 1997; Jürgens, 2005).

We show here that KN accumulates specifically in the Rab-A2/A3 compartment during mitosis and that RAB-A2 and -A3 proteins relocate along with KN to the growing margins of the cell plate. Notably, VHA-a1:GFP, which overlaps the Rab-A2/A3 compartment in interphase cells, was excluded from the cell plate, suggesting that the cell plate was related to the Rab-A2/A3 domain of the TGN/EE. Consistent with this, the Golgi, PVC, and GNOM compartments remained distinct from the Rab-A2/A3 compartment in dividing cells, and markers of these compartments were almost completely excluded from the cell plate. Furthermore, dominant mutants in RAB-A2^{a} strongly inhibited cytokinesis, resulting in enlarged binucleate and multinucleate cells and severe disruption of cell division patterns. The multinucleate cells must have completed several rounds of mitosis without cytokinesis, so the usual cell cycle checkpoints (Sollner et al., 2002) must have been passed repeatedly, suggesting that the RAB-A2^{a} mutants exerted a rather specific block on cytokinesis.

We propose that the Rab-A2/A3 TGN/EE compartment is the precursor to the cell plate and that the cell plate may even arise substantially by KN-mediated homotypic fusion of Rab-A2/A3–like membranes. Consistent with this, mutants of RAB-A2^{a} that stabilize the GDP- or GTP-bound state both localized to the growing margins of the cell plate, suggesting that they fulfilled their entire role there during cytokinesis.

It has been proposed that cell plate cargoes in BY-2 cells are stored in a Golgi-derived compartment before the onset of cytokinesis (Yasuhara et al., 1995; Yasuhara and Shibaoka, 2000; Jürgens and Pacher, 2004; Jürgens, 2005). In BY-2 cells, this compartment is BFA-insensitive, whereas the Rab-A2/A3 compartment in *Arabidopsis* root tips is BFA-sensitive. However, this difference may simply reflect the BFA sensitivity of the particular Arf-GEFs involved in each cell type (Richter et al., 2007; Teh and Moore, 2007), so these compartments may be equivalent.

Although the cell plate has been viewed as a compartment formed by post-Golgi biosynthetic traffic, this view has been challenged by the observation that it also accumulates endocytosed markers, including FM4-64 (Baluska et al., 2005; Dhonukshe et al., 2006). Therefore, it has been proposed that initiation and expansion of the cell plate occurs preferentially by aggregation of endosomes and not Golgi-localized endomembranes (Baluska et al., 2006; Dhonukshe et al., 2006). The endosomes responsible were proposed to be Rab-F2–positive multivesicular compartments, which were considered to be EEs (Ueda et al., 2004; Dhonukshe et al., 2006). Markers such as Rab-F2 and GNOM were localized to the cell plate, while Rab-F1, which overlaps Rab-F2, was shown to label KN-containing compartments in preprophase (Dhonukshe et al., 2006). However, the proposal that the cell plate is derived substantially from such endosomes is not easily reconciled with other evidence, such as electron tomography or the observation that the PVC markers SYP21 (At PEP12) and PI(3)P binding FYVE-GFP are absent from the cell plate (Muller et al., 2003; Segui-Simarro et al., 2004; Segui-Simarro and Staehelin, 2006; Vermeer et al., 2006).

Our observations can reconcile these differences. First, they strongly suggest that it is not the PVC but the earlier Rab-A2/A3 domain of the TGN/EE that provides membrane to the cell plate. This is consistent with the position of the Rab-A2/A3 domain as a

station on a pathway from the Golgi to the PM, an early site of FM4-64 and KN accumulation, and a major contributor to the cell plate. Thus, the arrival of FM4-64 at the cell plate along with Rab-A2/A3 membranes could be viewed as a modified recycling route from the TGN to the PM (Figures 7A, step 1, and 7D, step 2). The same pathway could deliver other recycling molecules as well as Golgi-derived biosynthetic cargo such as KN to the cell plate. A similar hypothesis has been made by Dettmer and colleagues (2006), but the TGN/EE marker they studied, VHA-a1, did not label the cell plate. The relative contribution of Golgi-derived and endocytosed molecules to the cell plate remains to be established.

Second, although we could confirm that there was some colocalization between KN and the PVC prior to cytokinesis, as reported by Dhonukshe and colleagues (2006), this was far less than for the Rab-A2/A3 compartment and may have resulted from the difficulty in resolving such closely juxtaposed compartments by immunofluorescence. Furthermore, we did not observe integral or peripheral markers of the PVC (GFP-BP80, mRFP1:RAB-F2^{b}, and YFP:RAB-F2^{a}) or the GNOM compartment (GNOM:GFP) on the cell plate. As GNOM:GFP complements the *gnom* mutant (Geldner et al., 2003; Geldner, 2004), this protein can fulfill its function without accumulating visibly at the cell plate. These differences between our observations and those of Dhonukshe and colleagues (2006) may be attributable to the use of different marker systems or to the use of live versus fixed cells, and this will need to be resolved by future work. Nevertheless, our observations highlight the present need for caution in the conclusion that endosomal and prevacuolar markers localize substantially and generally to the cell plate.

Finally, although dominant-negative RAB-F2^{b}[S24N] caused the appearance of binucleate cells in young seedlings (Dhonukshe et al., 2006), it is unclear whether cytokinesis displays equal sensitivity to mutants in RAB-F2 and RAB-A2. It is also unclear whether the requirement for Rab-F2 activity in cytokinesis arises from its function at the PVC or elsewhere (see above). We did not find tagged Rab-F2 proteins at the cell plate, so it may be that the Rab-F2 subclass has an indirect role in cell plate assembly. We note that, unlike the Rab-A2 and -A3 subclasses, RAB-F2^{b} and GNOM were not seen to concentrate at the growing margins of the cell plate by Dhonukshe and colleagues (2006) but were apparently distributed across the central region, where recycling occurs (Segui-Simarro et al., 2004; Segui-Simarro and Staehelin, 2006). Considering the need to rapidly turn over membrane and proteins such as KN (Lauber et al., 1997; Segui-Simarro et al., 2004; Jürgens, 2005; Segui-Simarro and Staehelin, 2006), one possibility is that the Rab-F2 subclass plays a role in traffic from the cell plate via the PVC (Figure 7D, step 3).

Rab-A Proteins in Plant and Animal Cytokinesis

The mechanisms of cytokinesis in plants and animals are superficially dissimilar, but increasing similarities are emerging at the molecular level with respect to cytoskeletal organization and membrane trafficking (Strickland and Burgess, 2004; Albertson et al., 2005; Otegui et al., 2005; Baluska et al., 2006). Our observations with the plant Rab-A proteins add a further parallel. The final stages of cytokinesis in animal cells require the addition of membrane to the cleavage furrow (Skop et al., 2001; Xu et al., 2002; Albertson et al., 2005; Yu et al., 2007). A key determinant of trafficking to the cleavage furrow is the Rab11 subclass (Pelissier et al., 2003; Riggs et al., 2003; Wilson et al., 2005; van IJzendoorn, 2006; Yu et al., 2007) that is paralogous to the plant Rab-A subclasses. This protein resides on the recycling endosome, where it is involved in recycling to the PM and also in traffic between the endosome and the TGN (Ullrich et al., 1996; Rodman and Wandinger-Ness, 2000; Wilcke et al., 2000; van IJzendoorn, 2006). During cytokinesis, however, new membrane is delivered specifically from the recycling endosome to the cleavage furrow to facilitate cell surface expansion. The parallels between Rab11 at the recycling endosome in dividing animal cells and the Rab-A subclasses at the Rab-A2/A3 compartment in plant cells are striking and suggest either convergence or ancient ancestry in the mechanisms of trafficking to the division plane. Interestingly, based on our own searches, the principal interactors of mammalian Rab11 during cytokinesis, including Rab11-FIPs and nuf (Hales et al., 2001; Riggs et al., 2003; Wilson et al., 2005; Grosshans et al., 2006; Yu et al., 2007), are apparently absent from plant genomes, suggesting that molecular activities of Rab-A proteins at the plant and mammalian division plane are likely to differ. It will be of interest to identify the proteins that interact with members of the plant Rab-A subclasses during cytokinesis.

METHODS

Molecular Cloning and Generation of YFP:Rab Fusions

Standard molecular techniques as described by Ausubel et al. (1999) were used to generate plasmids expressing YFP:Rab fusions. These were constructed in pBINPLUS (Vanengelen et al., 1995). The genomic fragments of At RabA genes were amplified from genomic DNA of wild-type *Arabidopsis thaliana* ecotype Columbia plants using the Expand High-Fidelity PCR system (Roche). Primers used to amplify the promoter regions and 5′ untranslated region of RAB-A2^{a}, RAB-A2^{b}, RAB-A2^{c}, RAB-A2^{d}, and RAB-A3 are 5′-CTTCTTTTAATTAAGTTTGCTTTTTCAGCAATTTT-3′ and 5′-CTTCTTGGTACCTGTTACACTTTTCTCGAGGA-3′, 5′-CTTCTTTTAATTAATAGCCAAGGTATACACCACTG-3′ and 5′-CTTCTTGGTACCTGCTTCTCAAATCCTAGCGTC-3′, 5′-CTTCTTCGATCGTTTTTTGATTGATTTGGTTAT-3′ and 5′-CTTCTTGGTACCTTTCTCCTTCTCTCTTCGATCTCGC-3′, 5′-CTTCTTTTAATTAACTTCGTCGTCGTCGTCGGCTT-3′ and 5′-CTTCTTGGTACCTTTTCCTCTTTGATCTCACCTATAAAC-3′, and 5′-CTTCTTTTAATTAATTGCTTCATCTCTTTCACCTC-3′ and 5′-CTTCTTGGTACCTATTGCGCTGATGAAGAAAACA-3′, respectively. The PCR product was digested and subcloned as a *Pac*I-*Acc*65I or *Pvu*I-*Acc*65I fragment into *Pac*I/*Acc*65I–digested pBINPLUS-*Pac*I-Promoter(Rab-C1)-*Acc*65I-GUS-*Asc*I (a gift of Steve Rutherford, University of Oxford), replacing the At RAB-C1 promoter and resulting in pBINPLUS-Promoter(Rab-A):GUS. To generate pBINPLUS-Promoter:YFP, the GUS fragment was then replaced by the *Acc*65I/*Asc*I–digested YFP-HA-linker fragment, which was amplified using 5′-ACACAAGGTACCATGGGATCCGTGAGCAAGGGCGAGGAGCTGTTCACC-3′ and 5′-CCTCCAGGCGCGCCAGCGTAATCTGGGTAATCGTAAGGATAGG-3′ from a vector containing Venus YFP (Nagai et al., 2002). Primers used to amplify the coding regions plus intron and 3′ regulatory sequences of Rab-A2^{a}, Rab-A2^{b}, Rab-A2^{c}, Rab-A2^{d}, and Rab-A3 are 5′-ACAAGGGCGCGCCTGGAGCAGGAATGGCGAGAAGACCGGACG-3′ and 5′-AACAAGGGCGCGCCAAGACTACCTTCTTCAGTCTTTGGA-3′,

5′-AACAAGGGCGCGCCTGGAGCAGGAATGGCGAATAGAATAGATC-ATGAG-3′ and 5′-AACAAGGGCGCGCCGAAAATAGATATCTGGCAA-CTGAG-3′, 5′-AACAAGGGCGCGCCTGGAGCAGGAATGACGCATAGA-GTAGAT-3′ and 5′-AACAAGGGCGCGCCATTAACTGAATTTATTTTTC-TAAAG-3′, 5′-AACAAGGGCGCGCCTGGAGCAGGAATGGCGCATAGG-GTAGAAC-3′ and 5′-AACAAGGGCGCGCCCCAACGAATTTCTGTGAT-GGCTGA-3′, and 5′-AACAAGGGCGCGCCTGGAGCAGGAATGAACGA-AGAGATGAGCGGTG-3′ and 5′-AACAAGGGCGCGCCGTTCAAAGAG-AACATTATGG-3′, respectively. The PCR product was digested and subcloned as a *Asc*I-*Asc*I fragment into *Asc*I-digested pBINPLUS-promoter:YFP, resulting in pBINPLUS-promoter:YFP:Rab. The sequences of coding regions were checked by sequencing.

Point mutations to generate the amino acid substitutions Ser-26 to Asn (S26N), Gln-71 to Leu (Q71L), and Asn-125 to Ile (N125I) were created by overlapping PCR using the Rab-A2^a genomic sequence in the plasmid pBINPLUSpromoter:YFP:Rab-A2^a as template. In the first round, two PCR products were obtained by amplifying the wild-type gene with one flanking primer and one mutagenized primer (primers 1 + 4 and 3 + 2; see below). These two fragments were combined and amplified with primers 1 + 2 to obtain the full-length mutagenized gene. The sequences of the primers used are as follows: primer 1, 5′-ACGCGTCGACCTCGAGTGGCGCGCCTG-GAGCAGGAATG-3′; primer 2, 5′-ACGGGGTACCGGCGCGCCAAGAC-TACCTTCTTC-3′. The restriction sites introduced by PCR and used for subcloning are underlined: *Sal*I, *Xho*I, *Asc*I, *Kpn*I, and *Asc*I. The primers used to induce mutation are as follows: QL primer 3, 5′-GACACAGCTGGG-TTAGAACGATACAGAGCCATAACTAG-3′; QL primer 4, 5′-TTCTAACC-CAGCTGTGTCCCATATCTGAGCTTTCAC-3′; SN primer 3, 5′-AAGAATA-ATCTCCTCAGTAGATTCACTCGCAACGAGTTC-3′; SN primer 4, 5′-TCT-ACTGAGGAGATTATTCTTGCCGACACCGGAGTC-3′; NI primer 3, 5′-GGG-ATCAAGACAGACCTTAAGCATCTCAGAGCAGTTGC-3′; NI primer 4, 5′-CTTAAGGTCTGTCTTGATCCCAATCAACATGATCACTATA-3′. The restriction sites introduced or removed by silent mutation are underlined and are, respectively, *Pvu*II, (*Xba*I), (*Bgl*II), and *Afl*II (sites in parentheses were removed). The Rab-A2^a mutated sequences were cloned as *Asc*I-*Asc*I fragments into the pBINPLUS-promoter:YFP:Rab-A2^a vector by replacement of the wild-type sequence by the mutated sequences. These sequences were also cloned as *Sal*I-*Kpn*I fragments into the pH-TOP vector (Craft et al., 2005) for dexamathasone-inducible expression.

Plant Material and Growth Conditions

Plants expressing Nag-EGFP or N-ST-YFP (Grebe et al., 2003) were a gift from Markus Grebe. The GFP:PsRAB-A3 (Pra2) (Inaba et al., 2002) construct was kindly made available by Yukiko Sasaki. Constructs of GFP-BP80, YFP:Rab-F2^a, and At GNOM:GFP (Geldner et al., 2003; Kotzer et al., 2004; Preuss et al., 2004) were kindly given by Chris Hawes, Erik Neilsen, and Gerd Jürgens, respectively. Constructs of mRFP1: Rab-F2^b and VHA-a1:GFP (Dettmer et al., 2006) were a gift from Karin Schumacher. Constructs were transformed into *Agrobacterium tumefaciens* C58 (GV3101) (Koncz and Schell, 1986) and then introduced into *Arabidopsis* ecotype Columbia plants by *Agrobacterium*-mediated transformation (Clough and Bent, 1998). Representative lines were selected from several independent transformants for further analyses. Coexpression of two fluorescent fusions was achieved by crossing (Koornneef et al., 1998) or transformation. Seeds were sterilized by 70% ethanol, allowed to imbibe for 2 to 4 d at 4°C, and germinated on vertically oriented agar plates containing Murashige and Skoog (MS) medium (pH 5.6 to 5.8). Sucrose (1%) was added sometimes to enhance the germination rate. Seedlings were grown at 22°C in a 16-h-light/8-h-dark regime. Experiments were performed on 5- to 12-d-old seedlings.

For dexamethasone-inducible expression, pH-TOP derivatives were introduced into the CaMV 35S LhGR driver line 4C-S5/7 (Craft et al., 2005). Transformants were selected by addition of hygromycin to plant culture medium at a concentration of 15 μg/mL (Calbiochem). For induction, T2 plants were germinated and grown on plates containing MS medium with 1.5% (w/v) sucrose supplemented with dexamethasone solution (20 μM) diluted from a 100 mM stock solution in DMSO or an equal volume of DMSO. Photographs were taken after 14 d using a Leica microscope (MZFLIII). The images were recorded with a Coolsnap digital camera (Roper Scientific).

Fluorescence Microscopy and Confocal Analysis

For fluorescence microscopy, seedlings on agar plates were analyzed with a Leica microscope (MZFLIII). The images were recorded with a Coolsnap digital camera (Roper Scientific). For confocal analysis, seedlings mounted in half-strength MS liquid (diluted in water) were analyzed with an upright Zeiss LSM 510 laser scanning microscope, using a 10× objective for low magnification imaging and either a C-apochromat 40×/1.2 numerical aperture water-immersion lens or a plan-apochromat 63×/1.4 numerical aperture oil-immersion lens for higher magnification images. All images were acquired using a line-sequential configuration. LSM software (Zeiss) was used for postacquisition image processing, including reconstruction of three-dimensional and four-dimensional images and adjustment of brightness and contrast. GFP or YPF were excited at 488 nm and detected with a 505- to 550-nm emission filter or LP505 nm. FM4-64, MitoTracker, or chlorophyll were excited at 488 or 543 nm and collected in a META detector by selecting a suitable range of spectrum. For multicolor imaging of GFP/YFP, GFP/YFP/FM4-64, or mRFP/FM4-64, signals were simultaneously collected by the META detector with eight activated individual channels and analyzed using the spectrum deconvolution function based on the reference spectra of each fluorophore. These eight channels covered 496 to 582 nm at 10.7-nm intervals for detecting GFP/YFP, 474 to 646 nm at 21.4-nm intervals for detecting GFP/YFP/FM4-64, and 576 to 651 nm at 10.7-nm intervals for detecting mRFP/FM4-64. To image YFP or GFP, DAPI (Sigma-Aldrich), and Cy3, DAPI (excited at 405 nm and detected with a 435- to 485-nm emission filter) and Cy3 (excited at 543 nm and detected with the 613- to 700-nm sensors of the META detector) were collected in one track while YFP/GFP was detected in another track with 488-nm excitation and a 505- to 550-nm filter. For multiple labeling, control samples, which gave only one type of fluorescent signal, were imaged to ensure that there was no bleed-through problem.

To image propidium iodide and Calcofluor simultaneously by confocal microscopy, propidium iodide was excited at 514 nm and collected in the 583- to 678-nm range of the META detector, while Calcofluor was detected with 405-nm excitation and a LP420 nm filter; excitation wavelengths were reflected using a 405/514 primary dichroic mirror, and emission wavelengths were separated with an NFT490 secondary dichroic mirror.

Fluorescent Dye and BFA Treatments

To visualize putative endosomes, seedlings were mounted in half-strength MS liquid with 5 μM FM4-64 (Invitrogen, Molecular Probes; T13320; diluted from a 5 mM stock in water) on slides for a specified time. To stain the mitochondria, seedlings were immersed in 0.2 μM MitoTracker Red CHXRos (Invitrogen, Molecular Probes; M7512; diluted from a 1 mM stock in DMSO) for 15 min prior to imaging. The seedlings were then mounted on slides with half-strength MS liquid for imaging. For BFA treatment, seedlings were incubated in half-strength MS liquid containing 25 to 50 μM BFA diluted from a 50 mM stock in DMSO and then mounted on the slides in the presence of BFA. To stain cell walls and nuclei, seedlings were immersed in a staining solution containing 35 μg/mL Calcofluor (diluted from a 3.5 mg/mL stock solution in 0.1 M Tris-HCl, pH 9), 200 μM $CaCl_2$, 10 μg/mL propidium iodide (diluted from a 1 mg/mL stock solution), 0.1% Triton, and

50 mM Tris, pH 8.0, and incubated on ice for 30 to 60 min prior to imaging. The seedlings were then mounted in the staining solution.

Protein Extraction and Protein Gel Blot Analysis

Protein extracts were prepared from roots of *Arabidopsis* seedlings (50 to 150 mg) frozen in liquid N_2. The tissue was ground in a microcentrifuge tube with a plastic pestle, followed by the addition of 2 volumes of the following extraction buffer: 50 mM sodium citrate, pH 5.5, 5% SDS (w/v), 0.01% BSA (w/v), 2% β-mercaptoethanol, 150 mM NaCl, and a protease inhibitor cocktail (Sigma-Aldrich; P2714; 17 μL per 500 mg of plant material). The mixture was boiled for 10 min and cleared by centrifugation at 12,500 rpm for 30 min at 4°C. The supernatant was transferred to a microcentrifuge tube, frozen in liquid N_2, and stored at −80°C until used.

SDS-PAGE was performed according to Sambrook et al. (1989) using a 12% polyacrylamide gel and a Protean III apparatus (Bio-Rad). Five to 10 μL of SeeBlue Plus 2 prestained standards (Invitrogen) was added as a protein ladder. After electrophoresis, proteins were transferred to a polyvinylidene difluoride membrane for 1.5 h in a transfer buffer according to Burnette (1981). The membrane was then blocked for 1 h in Tris-buffered saline containing 0.1% (v/v) Tween 20 (Sigma-Aldrich), 1% BSA (w/v) (fraction V; Roche Biochemicals), 0.1% goat serum (v/v), and 5% nonfat milk (w/v). An antibody to full-length GFP (Invitrogen, Molecular Probes; A6455) or an antibody raised against the Rab-A2^a C-terminal peptide (this work) was used at 1:1000 dilution to probe the membrane at 4°C overnight. Alkaline phosphatase–conjugated secondary antibody (Sigma-Aldrich) was used at 1:10,000 dilution (1 h of incubation at room temperature), and the results were determined with the Sigma-Aldrich fast 5-bromo-4-chloro-3-indolyl phosphate/nitroblue tetrazolium method, used according to the manufacturer's recommendations.

Immunofluorescence Localization

For whole-mount preparations, a protocol modified from Webb and Gunning (1990) and Goodbody and Lloyd (1994) was kindly made available by Sandra Richter and Gerd Jürgens. In brief, 5-d-old seedlings grown on MS agar without antibiotic were fixed in 4% paraformaldehyde in microtubule-stabilizing buffer (50 mM PIPES, 5 mM EGTA, and 5 mM $MgSO_4$, pH 6.9 to 7.0) at room temperature for 1 h. Vacuum was applied briefly at the beginning of the incubation for faster uptake. Seedlings were mounted on Menzel-Glaser positive-charged Superfrost Plus slides (Fisher Scientific). Cover slips were removed after dipping the slides into liquid nitrogen. After drying, specimens were rehydrated in PBS for 10 min. Cell walls were partially digested with 2% (w/v) driselase (Sigma-Aldrich) for 40 min at 37°C in a humid chamber. The PM was permeabilized with 10% DMSO and 1 to 3% IGEPAL (Sigma-Aldrich) in PBS for 1 h of incubation in a humid chamber at room temperate. Nonspecific interactions were blocked with 3% BSA in PBS at 37°C for 2 h. Blocking solution was then replaced by primary antibodies in blocking solution, and the slides were incubated for 1 to 1.5 h at 37°C followed by overnight incubation at 4°C. The slides were then incubated with fluorochrome-conjugated secondary antibodies in a humid chamber in the dark at 37°C for 3.5 h. Washing steps were performed with PBS for 10 min four to six times. DAPI (1 μg/mL in PBS; Sigma-Aldrich) staining was performed for 10 min between the fifth and sixth washing steps following secondary antibody incubation. One to two drops of antifading solution (Citifluor glycerol/PBS solution AF1; Agar Scientific) were added to the specimen, and cover slips were placed. The slides were stored at 4°C for up to 1 week before CLSM. Primary antibodies were used at the following concentrations: anti-KN (a kind gift from Gerd Jürgens), 1:4000; anti-PIN1 (a kind gift from Gerd Jürgens), 1:200; anti-α-tubulin (Abcam; ab6160), 1:600; anti-Rab-A2^a, 1:3000 to 1:6000. Secondary antibodies were used at the following concentrations: fluorescein isothiocyanate–conjugated AffiniPure anti-rat IgG (Jackson ImmunoResearch; 112-095-167), 1:150; fluorescein isothiocyanate–conjugated AffiniPure F(ab′)$_2$ fragment anti-rabbit IgG (Jackson ImmunoResearch; 111-096-144), 1:150; Cy3-conjugated AffiniPure anti-rabbit IgG (Jackson ImmunoResearch; 11-165-144), 1:600; Cy3-conjugated AffiniPure anti-rat IgG (Jackson ImmunoResearch; 112-165-143), 1:600; and Cy3-conjugated AffiniPure anti-mouse IgG (Jackson ImmunoResearch; 115-165-146); 1:600.

Generation of RAB-A2^a–Specific Antibody

A C-terminal peptide specific to Rab-A2^a (KEGQTIDVAATSESNAKKPC) was synthesized (Harlan Serlab) and used for immunization of rabbits and the subsequent ELISA tests (Harlan Serlab). The antiserum was then purified by SulfoLink column, which had been coupled with the Rab-A2^a peptide (2 mg of peptide to 1 mL of SulfoLink coupling gel) according to the manufacturer's instructions (Pierce). The bound antibodies were eluted with Gly buffer (100 mM, pH 2.5 to 3.0). The elution was then neutralized by 1 M Tris-HCl (pH 7.5), and the buffer was exchanged with PBS using Zeba Desalt spin columns (Pierce) according to the manufacturer's instructions. The antibody was further purified by passage through a Sulfolink column bearing an unrelated peptide sequence and collection of the flow-through.

Accession Numbers

Sequence data from this article can be found in the Arabidopsis Genome Initiative or GenBank/EMBL databases under the following accession numbers: At *RAB-A2^a*, At1g09630; At *RAB-A2^b*, At1g07410; At *RAB-A2^c*, At3g46830; At *RAB-A2^d*, At5g59150; At *RAB-A3*, At1g01200; KNOLLE (At SYP111), At1g08560; Pra2/PsRAB-A3, AB007911; At *RAB-B1^b*, At4g17170; At *RAB-C1*, At1g43890; At *RAB-E1^d*, At5g03520; At *RAB-F2^a*, At 5g45130; At *RAB-F2^b*, At4g19640; At *RAB-H1^d*/At *RAB6*, At2g22290.

Supplemental Data

The following materials are available in the online version of this article.

Supplemental Figure 1. Genomic DNA Fragments of Rab-A Genes Used for the Construction of YFP Fusions.

Supplemental Figure 2. YFP Fluorescence of YFP-Tagged Genomic Fusions of All Members of the *Arabidopsis* Rab-A2 and Rab-A3 Group.

Supplemental Figure 3. Histograms of Expression Levels of Members of the Rab-A2 and -A3 Subclasses in *Arabidopsis* Plants Extracted from the Developmental Data Sets of AtGenExpress.

Supplemental Figure 4. RAB-A2 and PsRAB-A3 Label the Same Compartment.

Supplemental Figure 5. xFP:RAB-A–Labeled Compartments Are Distinct from the Golgi.

Supplemental Figure 6. YFP:RAB-A–Labeled Compartments Are Distinct from the GFP-BP80–Labeled PVC.

Supplemental Figure 7. xFP:RAB-A–Labeled Compartments Are Rapidly Labeled by FM4-64, while Compartments Labeled by xFP fusions to RAB-E1^c, RAB-F2, or GNOM Are Labeled Inefficiently by FM4-64.

Supplemental Figure 8. FM4-64 Labels GFP-BP80 Compartments Less Efficiently Than the YFP:RAB-A2/A3 Compartment.

Supplemental Figure 9. Time Series Analysis of FM4-64 Labeling of the Rab-A2/A3 Compartment.

Supplemental Figure 10. Rapid Relocation of YFP:RAB-A2 and -A3 to BFA Bodies in *Arabidopsis* Root Tips.

Supplemental Figure 11. Subcellular Compartments of *Arabidopsis* Root Tip Epidermal Cells Respond Differently to BFA Treatment.

Supplemental Figure 12. RAB-A2/A3 Target xFP to Cell Plate–Like Structures, Which Are Rapidly Labeled with FM4-64.

Supplemental Figure 13. Tagged RAB-A2/A3 Proteins Localized to Cell Plates, Which Were Sandwiched by the Phragmoplast and Colabeled by KN.

Supplemental Figure 14. Labeling Patterns of YFP:RAB-A2–Labeled Cell Plates Change over Time, as Shown by the Time Series of Three-Dimensional Images Reconstructed from Serial Sections.

Supplemental Figure 15. xFP:RAB-A2/A3 Localized to KN-Positive Structures before the Onset of Cytokinesis.

Supplemental Figure 16. YFP:RAB-A2/A3–Labeled Compartments and mRFP:RAB-F2^{b}–Labeled Compartments Remain Distinct during Cytokinesis.

Supplemental Figure 17. Cell Plate Localization Is Not a General Feature of xFP:RAB Fusions.

Supplemental Figure 18. YFP:RAB-A2^{a}[N125I] Labels FM4-64–Positive Endosomes.

Supplemental Figure 19. Inducible Expression from the CaMV35S:LhGR Activator Line 4c Is Weaker in the Meristematic Region of the Root.

Supplemental Movie 1. Four-Dimensional Analysis of YFP:RAB-A2^{d} in a Lateral Root Tip Showing Several Cytokinesis Events.

ACKNOWLEDGMENTS

We thank Karin Schumacher, Toru Fujiwara, Gerd Jürgens, Marcus Grebe, Niko Geldner, Ulla Neumann, Steve Rutherford, and Chris Hawes for plasmids, antibodies, or seeds of marker lines. This work was supported by a Croucher Foundation Scholarship to C.-M.C. and by Biotechnology and Biological Science Research Council Grants BB/D004055/1 and 43/REI20537 to I.M.

Received April 2, 2007; revised December 10, 2007; accepted January 13, 2008; published January 31, 2008.

REFERENCES

Albertson, R., Riggs, B., and Sullivan, W. (2005). Membrane traffic: A driving force in cytokinesis. Trends Cell Biol. **15:** 92–101.

Anai, T., Hasegawa, K., Watanabe, Y., Uchimiya, H., Ishizaki, R., and Matsui, M. (1991). Isolation and analysis of cDNAs encoding small GTP-binding proteins of *Arabidopsis thaliana.* Gene **108:** 259–264.

Ausubel, F., Brent, R., Kingston, R.E., Moore, J.G., Seidman, J.G., Smith, J.A., and Struhl, J.G. (1999). Current Protocols in Molecular Biology. (New York: John Wiley & Sons).

Baluska, F., Liners, F., Hlavacka, A., Schlicht, M., Van Cutsem, P., McCurdy, D.W., and Menzel, D. (2005). Cell wall pectins and xyloglucans are internalized into dividing root cells and accumulate within cell plates during cytokinesis. Protoplasma **225:** 141–155.

Baluska, F., Menzel, D., and Barlow, P.W. (2006). Cytokinesis in plant and animal cells: Endosomes 'shut the door.' Dev. Biol. **294:** 1–10.

Batoko, H., Zheng, H.Q., Hawes, C., and Moore, I. (2000). A rab1 GTPase is required for transport between the endoplasmic reticulum and Golgi apparatus and for normal Golgi movement in plants. Plant Cell **12:** 2201–2218.

Bednarek, S.Y., and Falbel, T.G. (2002). Membrane trafficking during plant cytokinesis. Traffic **3:** 621–629.

Bloch, D., Lavy, M., Efrat, Y., Efroni, I., Bracha-Drori, K., Abu-Abied, M., Sadot, E., and Yalovsky, S. (2005). Ectopic expression of an activated RAC in Arabidopsis disrupts membrane cycling. Mol. Biol. Cell **16:** 1913–1927.

Boevink, P., Oparka, K., Cruz, S.S., Martin, B., Betteridge, A., and Hawes, C. (1998). Stacks on tracks: The plant Golgi apparatus traffics on an actin/ER network. Plant J. **15:** 441–447.

Bolte, S., Talbot, C., Boutte, Y., Catrice, O., Read, N.D., and Satiat-Jeunemaitre, B. (2004). FM-dyes as experimental probes for dissecting vesicle trafficking in living plant cells. J Microsc. **214:** 159–173.

Burnette, W.N. (1981). Western blotting: Electrophoretic transfer of proteins from sodium dodecyl sulfate polyacrylamide gels to unmodified nitrocellulose and radiographic detection with antibody and radioiodinated protein A. Anal. Biochem. **112:** 195–203.

Chen, S.H., Chen, S., Tokarev, A.A., Liu, F.L., Jedd, G., and Segev, N. (2005). Ypt31/32 GTPases and their novel F-box effector protein Rcy1 regulate protein recycling. Mol. Biol. Cell **16:** 178–192.

Cheng, H., Sugiura, R., Wu, W.L., Fujita, M., Lu, Y.B., Sio, S.O., Kawai, R., Takegawa, K., Shuntoh, H., and Kuno, T. (2002). Role of the rab GTP-binding protein Ypt3 in the fission yeast exocytic pathway and its connection to calcineurin function. Mol. Biol. Cell **13:** 2963–2976.

Cheung, A.Y., Chen, C.Y.H., Glaven, R.H., de Graaf, B.H.J., Vidali, L., Hepler, P.K., and Wu, H.M. (2002). Rab2 GTPase regulates vesicle trafficking between the endoplasmic reticulum and the Golgi bodies and is important to pollen tube growth. Plant Cell **14:** 945–962.

Clough, S.J., and Bent, A.F. (1998). Floral dip: A simplified method for *Agrobacterium*-mediated transformation of *Arabidopsis thaliana.* Plant J. **16:** 735–743.

Craft, J., Samalova, M., Baroux, C., Townley, H., Martinez, A., Jepson, I., Tsiantis, M., and Moore, I. (2005). New pOp/LhG4 vectors for stringent glucocorticoid-dependent transgene expression in Arabidopsis. Plant J. **41:** 899–918.

daSilva, L.L.P., Foresti, O., and Denecke, J. (2006). Targeting of the plant vacuolar sorting receptor BP80 is dependent on multiple sorting signals in the cytosolic tail. Plant Cell **18:** 1477–1497.

daSilva, L.L.P., Taylor, J.P., Hadlington, J.L., Hanton, S.L., Snowden, C.J., Fox, S.J., Foresti, O., Brandizzi, F., and Denecke, J. (2005). Receptor salvage from the prevacuolar compartment is essential for efficient vacuolar protein targeting. Plant Cell **17:** 132–148.

de Graaf, B.H.J., Cheung, A.Y., Andreyeva, T., Levasseur, K., Kieliszewski, M., and Wu, H.M. (2005). Rab11 GTPase-regulated membrane trafficking is crucial for tip-focused pollen tube growth in tobacco. Plant Cell **17:** 2564–2579.

Dettmer, J., Hong-Hermesdorf, A., Stierhof, Y.D., and Schumacher, K. (2006). Vacuolar H^{+}-ATPase activity is required for endocytic and secretory trafficking in Arabidopsis. Plant Cell **18:** 715–730.

Dhonukshe, P., Aniento, F., Hwang, I., Robinson, D.G., Mravec, J., Stierhof, Y.-D., and Friml, J. (2007). Clathrin-mediated constitutive endocytosis of PIN auxin efflux carriers in Arabidopsis. Curr. Biol. **17:** 520–527.

Dhonukshe, P., Baluska, F., Schlicht, M., Hlavacka, A., Samaj, J., Friml, J., and Gadella, T.W.J. (2006). Endocytosis of cell surface material mediates cell plate formation during plant cytokinesis. Dev. Cell **10:** 137–150.

Friml, J., Wisniewska, J., Benkova, E., Mendgen, K., and Palme, K. (2002). Lateral relocation of auxin efflux regulator PIN3 mediates tropism in Arabidopsis. Nature **415:** 806–809.

Geldner, N. (2004). The plant endosomal system—Its structure and role in signal transduction and plant development. Planta **219:** 547–560.

Geldner, N., Anders, N., Wolters, H., Keicher, J., Kornberger, W., Muller, P., Delbarre, A., Ueda, T., Nakano, A., and Jürgens, G. (2003). The Arabidopsis GNOM ARF-GEF mediates endosomal recycling, auxin transport, and auxin-dependent plant growth. Cell **112:** 219–230.

Goodbody, K.C., and Lloyd, C.W. (1994). Immunofluorescence techniques for analysis of the cytoskeleton. In Plant Cell Biology. A Practical Approach, N. Harris and K.J. Oparka, eds (Oxford, UK: IRL Press), pp. 221–243.

Grebe, M., Friml, J., Swarup, R., Ljung, K., Sandberg, G., Terlou, M., Palme, K., Bennett, M.J., and Scheres, B. (2002). Cell polarity signaling in Arabidopsis involves a BFA-sensitive auxin influx pathway. Curr. Biol. **12:** 329–334.

Grebe, M., Xu, J., Mobius, W., Ueda, T., Nakano, A., Geuze, H.J., Rook, M.B., and Scheres, B. (2003). Arabidopsis sterol endocytosis involves actin-mediated trafficking via ARA6-positive early endosomes. Curr. Biol. **13:** 1378–1387.

Grosshans, B.L., Ortiz, D., and Novick, P. (2006). Rabs and their effectors: Achieving specificity in membrane traffic. Proc. Natl. Acad. Sci. USA **103:** 11821–11827.

Gruenberg, J., and Stenmark, H. (2004). Opinion: The biogenesis of multivesicular endosomes. Nat. Rev. Mol. Cell Biol. **5:** 317–323.

Haas, T.J., Sliwinski, M.K., Martinez, D.E., Preuss, M., Ebine, K., Ueda, T., Nielsen, E., Odorizzi, G., and Otegui, M. (2007). The Arabidopsis AAA ATPase SKD1 is involved in multivesicular endosome function and interacts with its positive regulator LYST-INTERACTING PROTEIN5. Plant Cell **19:** 1295–1312.

Hales, C.M., Griner, R., Hobdy-Henderson, K.C., Dorn, M.C., Hardy, D., Kumar, R., Navarre, J., Chan, E.K.L., Lapierre, L.A., and Goldenring, J.R. (2001). Identification and characterization of a family of Rab11-interacting proteins. J. Biol. Chem. **276:** 39067–39075.

Harsay, E., and Schekman, R. (2002). A subset of yeast vacuolar protein sorting mutants is blocked in one branch of the exocytic pathway. J. Cell Biol. **156:** 271–285.

Heo, J.B., Rho, H.S., Kim, S.W., Hwang, S.M., Kwon, H.J., Nahm, M.Y., Bang, W.Y., and Bahk, J.D. (2005). OsGAP1 functions as a positive regulator of OsRab11-mediated TGN to PM or vacuole trafficking. Plant Cell Physiol. **46:** 2005–2018.

Inaba, T., Nagano, Y., Nagasaki, T., and Sasaki, Y. (2002). Distinct localization of two closely related Ypt3/Rab11 proteins on the trafficking pathway in higher plants. J. Biol. Chem. **277:** 9183–9188.

Jaillais, Y., Fobis-Loisy, I., Miege, C., Rollin, C., and Gaude, T. (2006). AtSNX1 defines an endosome for auxin-carrier trafficking in Arabidopsis. Nature **443:** 106–109.

Jaillais, Y., Santambrogio, M., Rozier, F., Fobis-Loisy, I., Miège, C., and Gaude, T. (2007). The retromer protein VPS29 links cell polarity and organ initiation in plants. Cell **130:** 1057–1070.

Jedd, G., Mulholland, J., and Segev, N. (1997). Two new Ypt GTPases are required for exit from the yeast trans-Golgi compartment. J. Cell Biol. **137:** 563–580.

Jones, S., Litt, R.J., Richardson, C.J., and Segev, N. (1995). Requirement of nucleotide exchange factor for Ypt1 GTPase mediated protein transport. J. Cell Biol. **130:** 1051–1061.

Jürgens, G. (2004). Membrane trafficking in plants. Annu. Rev. Cell Dev. Biol. **20:** 481–504.

Jürgens, G. (2005). Plant cytokinesis: Fission by fusion. Trends Cell Biol. **15:** 277–283.

Jürgens, G., and Pacher, T. (2004). Cytokinesis: Membrane trafficking by default? In The Golgi Apparatus and the Plant Secretory Pathways, D.G. Robinson, ed (Oxford, UK: Blackwell), pp. 238–254.

Kane, P.M. (2006). The where, when, and how of organelle acidification by the yeast vacuolar H^+-ATPase. Microbiol. Mol. Biol. Rev. **70:** 177–191.

Koncz, C., and Schell, J. (1986). The promoter of Tl-DNA gene 5 controls the tissue-specific expression of chimeric genes carried by a novel type of Agrobacterium binary vector. Mol. Gen. Genet. **204:** 383–396.

Koornneef, M., Alonso-Blanco, C., and Stam, P. (1998). Genetic analysis. In Arabidopsis Protocol (Totawa, NJ: Humana Press), pp. 105–118.

Kotzer, A.M., Brandizzi, F., Neumann, U., Paris, N., Moore, I., and Hawes, C. (2004). AtRabF2b (Ara7) acts on the vacuolar trafficking pathway in tobacco leaf epidermal cells. J. Cell Sci. **117:** 6377–6389.

Lauber, M.H., Waizenegger, I., Steinmann, T., Schwarz, H., Mayer, U., Hwang, I., Lukowitz, W., and Jürgens, G. (1997). The *Arabidopsis* KNOLLE protein is a cytokinesis-specific syntaxin. J. Cell Biol. **139:** 1485–1493.

Lam, S.K., Siu, C.L., Hillmer, S., Jang, S., An, G., Robinson, D.G., and Jiang, L. (2007a). Rice SCAMP1 defines clathrin-coated trans-Golgi-located tubular-vesicular structures as an early endosome in tobacco BY-2 cells. Plant Cell **19:** 296–319.

Lam, S.K., Tse, Y.C., Robinson, D.G., and Jiang, L. (2007b). Tracking down the elusive early endosome. Trends Plant Sci. **12:** 497–505.

Lee, G.J., Sohn, E.J., Lee, M.H., and Hwang, I. (2004). The Arabidopsis Rab5 homologs Rha1 and Ara7 localize to the prevacuolar compartment. Plant Cell Physiol. **45:** 1211–1220.

Marcote, M.J., Gu, F., Gruenberg, J., and Aniento, F. (2000). Membrane transport in the endocytic pathway: Animal versus plant cells. Protoplasma **210:** 123–132.

Miao, Y., Yan, P.K., Kim, H., Hwang, I., and Jiang, L. (2006). Localization of green fluorescent protein fusions with the seven Arabidopsis vacuolar sorting receptors to prevacuolar compartments in tobacco BY-2 cells. Plant Physiol. **142:** 945–962.

Moore, I. (2002). Gravitropism: Lateral thinking in auxin transport. Curr. Biol. **12:** R452–R454.

Mouratou, B., Biou, V., Joubert, A., Cohen, J., Shields, D.J., Geldner, N., Jürgens, G., Melancon, P., and Cherfils, J. (2005). The domain architecture of large guanine nucleotide exchange factors for the small GTP-binding protein Arf. BMC Genomics **6:** 20

Muller, I., Wagner, W., Volker, A., Schellmann, S., Nacry, P., Kuttner, F., Schwarz-Sommer, Z., Mayer, U., and Jürgens, G. (2003). Syntaxin specificity of cytokinesis in Arabidopsis. Nat. Cell Biol. **5:** 531–534.

Munro, S. (2004). Organelle identity and the organization of membrane traffic. Nat. Cell Biol. **6:** 469–472.

Nagai, T., Ibata, K., Park, E.S., Kubota, M., Mikoshiba, K., and Miyawaki, A. (2002). A variant of yellow fluorescent protein with fast and efficient maturation for cell-biological applications. Nat. Biotechnol. **20:** 87–90.

Oliviusson, P., Heinzerling, O., Hillmer, S., Hinz, G., Tse, Y.C., Jiang, L., and Robinson, D.G. (2006). Plant retromer, localized to the prevacuolar compartment and microvesicles in Arabidopsis, may interact with vacuolar sorting receptors. Plant Cell **18:** 1239–1252.

Olkkonen, V.M., and Stenmark, H. (1997). Role of Rab GTPases in membrane traffic. Int. Rev. Cytol. **176:** 1–85.

Ortiz, D., and Novick, P.J. (2006). Ypt32p regulates the translocation of Chs3p from an internal pool to the plasma membrane. Eur. J. Cell Biol. **85:** 107–116.

Otegui, M.S., Herder, R., Schulze, J., Jung, R., and Staehelin, L.A. (2006). The proteolytic processing of seed storage proteins in Arabidopsis embryo cells starts in the multivesicular bodies. Plant Cell **18:** 2567–2581.

Otegui, M.S., Verbrugghe, K.J., and Skop, A.R. (2005). Midbodies and phragmoplasts: Analogous structures involved in cytokinesis. Trends Cell Biol. **15:** 404–413.

Pelham, H.R. (2002). Insights from yeast endosomes. Curr. Opin. Cell Biol. **14:** 454–462.

Pelissier, A., Chauvin, J.P., and Lecuit, T. (2003). Trafficking through Rab11 endosomes is required for cellularization during Drosophila embryogenesis. Curr. Biol. **13:** 1848–1857.

Pereira-Leal, J.B., and Seabra, M.C. (2001). Evolution of the Rab family of small GTP-binding proteins. J. Mol. Biol. **313:** 889–901.

Pfeffer, S.R. (2001). Rab GTPases: Specifying and deciphering organelle identity and function. Trends Cell Biol. **11:** 487–491.

Prescianotto-Baschong, C., and Riezman, H. (2002). Ordering of compartments in the yeast endocytic pathway. Traffic **3:** 37–49.

Preuss, M.L., Schmitz, A.J., Thole, J.M., Bonner, H.K.S., Otegui, M.S., and Nielsen, E. (2006). A role for the RabA4b effector protein PI-4Kβ1 in polarized expansion of root hair cells in *Arabidopsis thaliana.* J. Cell Biol. **172:** 991–998.

Preuss, M.L., Serna, J., Falbel, T.G., Bednarek, S.Y., and Nielsen, E. (2004). The Arabidopsis Rab GTPase RabA4b localizes to the tips of growing root hair cells. Plant Cell **16:** 1589–1603.

Proikas-Cezanne, T., Gaugel, A., Frickey, T., and Nordheim, A. (2006). Rab14 is part of the early endosomal clathrin-coated TGN microdomain. FEBS Lett. **580:** 5241–5246.

Record, R.D., and Griffing, L.R. (1988). Convergence of the endocytic and lysosomal pathways in soybean protoplasts. Planta **176:** 425–432.

Richter, S., Geldner, N., Schrader, J., Wolters, H., Stierhof, Y.D., Rios, G., Koncz, C., Robinson, D.G., and Jürgens, G. (2007). Functional diversification of closely related ARF-GEFs in protein secretion and recycling. Nature **448:** 488–492.

Riggs, B., Rothwell, W., Mische, S., Hickson, G.R.X., Matheson, J., Hays, T.S., Gould, G.W., and Sullivan, W. (2003). Actin cytoskeleton remodeling during early Drosophila furrow formation requires recycling endosomal components Nuclear-fallout and Rab11. J. Cell Biol. **163:** 143–154.

Rodman, J.S., and Wandinger-Ness, A. (2000). Rab GTPases coordinate endocytosis—Commentary. J. Cell Sci. **113:** 183–192.

Russinovaa, E., Borst, J.W., Kwaaitaal, M., Cano-Delgado, A., Yin, Y.H., Chory, J., and de Vries, S.C. (2004). Heterodimerization and endocytosis of Arabidopsis brassinosteroid receptors BRI1 and AtSERK3 (BAK1). Plant Cell **16:** 3216–3229.

Rutherford, S., and Moore, I. (2002). The Arabidopsis Rab GTPase family: Another enigma variation. Curr. Opin. Plant Biol. **5:** 518–528.

Samalova, M., Fricker, M., and Moore, I. (2006). Ratiometric fluorescence-imaging assays of plant membrane traffic using polyproteins. Traffic **7:** 1701–1723.

Sambrook, J., Fritsch, E.F., and Maniatis, T. (1989). Molecular Cloning: A Laboratory Manual. (Cold Spring Harbor, NY: Cold Spring Harbor Laboratory Press).

Sanderfoot, A.A., Assaad, F.F., and Raikhel, N.V. (2000). The Arabidopsis genome. An abundance of soluble N-ethylmaleimide-sensitive factor adaptor protein receptors. Plant Physiol. **124:** 1558–1569.

Schmid, M., Davison, T.S., Henz, S.R., Pape, U.J., Demar, M., Vingron, M., Scholkopf, B., Weigel, D., and Lohmann, J.U. (2005). A gene expression map of *Arabidopsis thaliana* development. Nat. Genet. **37:** 501–506.

Schmitt, H.D., Wagner, P., Pfaff, E., and Gallwitz, D. (1986). The ras-related YPT1 gene product in yeast: A GTP-binding protein that might be involved in microtubule organization. Cell **47:** 401–412.

Seabra, M.C., and Wasmeier, C. (2004). Controlling the location and activation of Rab GTPases. Curr. Opin. Cell Biol. **16:** 451–457.

Segev, N. (2001). Ypt/Rab GTPases: Regulators of protein trafficking. Sci. STKE **100:** 1–18.

Segui-Simarro, J.M., Austin, J.R., White, E.A., and Staehelin, L.A. (2004). Electron tomographic analysis of somatic cell plate formation in meristematic cells of Arabidopsis preserved by high-pressure freezing. Plant Cell **16:** 836–856.

Segui-Simarro, J.M., and Staehelin, L.A. (2006). Cell cycle-dependent changes in Golgi stacks, vacuoles, clathrin-coated vesicles and multivesicular bodies in meristematic cells of *Arabidopsis thaliana*: A quantitative and spatial analysis. Planta **223:** 223–236.

Sipos, G., Brickner, J.H., Brace, E.J., Chen, L., Rambourg, A., Kepes, F., and Fuller, R.S. (2004). Soi3p/Rav1p functions at the early endosome to regulate endocytic trafficking to the vacuole and localization of trans-Golgi network transmembrane proteins. Mol. Biol. Cell **15:** 3196–3209.

Skop, A.R., Bergmann, D., Mohler, W.A., and White, J.G. (2001). Completion of cytokinesis in *C. elegans* requires a brefeldin A-sensitive membrane accumulation at the cleavage furrow apex. Curr. Biol. **11:** 735–746.

Sohn, E.J., Kim, S.E., Zhao, M., Kim, S.J., Kim, H., Kim, Y.-W., Lee, Y.J., Hillmer, S., Sohn, U., Jiang, L., and Hwang, I. (2003). Rha1, an Arabidopsis Rab5 homolog, plays a critical role in the vacuolar trafficking of soluble cargo proteins. Plant Cell **15:** 1057–1070.

Sollner, R., Glasser, G., Wanner, G., Somerville, C.R., Jürgens, G., and Assaad, F.F. (2002). Cytokinesis-defective mutants of Arabidopsis. Plant Physiol. **129:** 678–690.

Steinmann, T., Geldner, N., Grebe, M., Mangold, S., Jackson, C.L., Paris, S., Galweiler, L., Palme, K., and Jürgens, G. (1999). Coordinated polar localization of auxin efflux carrier PIN1 by GNOM ARF GEF. Science **286:** 316–318.

Strickland, L.I., and Burgess, D.R. (2004). Pathways for membrane trafficking during cytokinesis. Trends Cell Biol. **14:** 115–118.

Takano, J., Miwa, K., Yuan, L.X., von Wiren, N., and Fujiwara, T. (2005). Endocytosis and degradation of BOR1, a boron transporter of *Arabidopsis thaliana*, regulated by boron availability. Proc. Natl. Acad. Sci. USA **102:** 12276–12281.

Tanchak, M.A., Rennie, P.J., and Fowke, L.C. (1988). Ultrastructure of the partially coated reticulum and dictyosomes during endocytosis by soybean protoplasts. Planta **175:** 433–441.

Teh, O.K., and Moore, I. (2007). An ARF-GEF acting at the Golgi and in selective endocytosis in polarized plant cells. Nature **448:** 493–496.

Tse, Y.C., Mo, B.X., Hillmer, S., Zhao, M., Lo, S.W., Robinson, D.G., and Jiang, L.W. (2004). Identification of multivesicular bodies as prevacuolar compartments in *Nicotiana tabacum* BY-2 cells. Plant Cell **16:** 672–693.

Ueda, T., Anai, T., Tsukaya, H., Hirata, A., and Uchimiya, H. (1996). Characterization and subcellular localization of a small GTP-binding protein (Ara-4) from Arabidopsis: Conditional expression under control of the promoter of the gene for heat-shock protein HSP81-1. Mol. Gen. Genet. **250:** 533–539.

Ueda, T., Uemura, T., Sato, M.H., and Nakano, A. (2004). Functional differentiation of endosomes in Arabidopsis cells. Plant J. **40:** 783–789.

Ueda, T., Yamaguchi, M., Uchimiya, H., and Nakano, A. (2001). Ara6, a plant-unique novel type Rab GTPase, functions in the endocytic pathway of *Arabidopsis thaliana.* EMBO J. **20:** 4730–4741.

Ullrich, O., Reinsch, S., Urbe, S., Zerial, M., and Parton, R.G. (1996). Rab11 regulates recycling through the pericentriolar recycling endosome. J. Cell Biol. **135:** 913–924.

Vanengelen, F.A., Molthoff, J.W., Conner, A.J., Nap, J.P., Pereira, A., and Stiekema, W.J. (1995). pBINPLUS—An improved plant transformation vector based on pBIN19. Transgenic Res. **4:** 288–290.

van IJzendoorn, S.C. (2006). Recycling endosomes. J. Cell Sci. **119:** 1679–1681.

Vermeer, J.E.M., van Leeuwen, W., Tobena-Santamaria, R., Laxalt, A.M., Jones, D.M., Divech, N., Gadella, T.W.J., Jr., and Munnik, T. (2006). Visualisation of PtdIns3P dynamics in living plant cells. Plant J. **47:** 687–700.

Vernoud, V., Horton, A.C., Yang, Z., and Nielsen, E. (2003). Analysis of the small GTPase gene superfamily of Arabidopsis. Plant Physiol. **131:** 1191–1208.

Webb, M.C., and Gunning, B.E.S. (1990). Embryo sac development in *Arabidopsis thaliana*. I. Megasporogenesis, including the microtubular cytoskeleton. Sex. Plant Reprod. **3:** 244–256.

Wilcke, M., Johannes, L., Galli, T., Mayau, V., Goud, B., and Salamero, J. (2000). Rab11 regulates the compartmentalization of early endosomes required for efficient transport from early endosomes to the trans-Golgi network. J. Cell Biol. **151:** 1207–1220.

Wilson, G.M., Fielding, A.B., Simon, G.C., Yu, X., Andrews, P.D., Hames, R.S., Frey, A.M., Peden, A.A., Gould, G.W., and Pekeris, R. (2005). The FIP3-Rab11 protein complex regulates recycling endosome targeting to the cleavage furrow during late cytokinesis. Mol. Biol. Cell **16:** 849–860.

Xu, H., Boulianne, G.L., and Trimble, W.S. (2002). Membrane trafficking in cytokinesis. Semin. Cell Dev. Biol. **13:** 77–82.

Yamada, K., Fuji, K., Shimada, T., Nishimura, M., and Hara-Nishimura, I. (2005). Endosomal proteases facilitate the fusion of endosomes with vacuoles at the final step of the endocytotic pathway. Plant J. **41:** 888–898.

Yasuhara, H., and Shibaoka, H. (2000). Inhibition of cell-plate formation by brefeldin A inhibited the depolymerization of microtubules in the central region of the phragmoplast. Plant Cell Physiol. **41:** 300–310.

Yasuhara, H., Sonobe, S., and Shibaoka, H. (1995). Effects of brefeldin-A on the formation of the cell plate in tobacco BY-2 cells. Eur. J. Cell Biol. **66:** 274–281.

Yu, X., Prekeris, R., and Gould, G.W. (2007). Role of endosomal Rab GTPases in cytokinesis. Eur. J. Cell Biol. **86:** 25–35.

Zerial, M., and McBride, H. (2001). Rab proteins as membrane organizers. Nat. Rev. Mol. Cell Biol. **2:** 107–117.

Zheng, H., Camacho, L., Wee, E., Batoko, H., Legen, J., Leaver, C.J., Malho, R., Hussey, P.J., and Moore, I. (2005). A Rab-E GTPase mutant acts downstream of the Rab-D subclass in biosynthetic membrane traffic to the plasma membrane in tobacco leaf epidermis. Plant Cell **17:** 2020–2036.

Zheng, H.Q., Kunst, L., Hawes, C., and Moore, I. (2004). A GFP-based assay reveals a role for RHD3 in transport between the endoplasmic reticulum and Golgi apparatus. Plant J. **37:** 398–414.